

# Strong and weak lensing of Gravitational Waves: a semi-analytical approach

Giulia Cusin<sup>a</sup> Ruth Durrer<sup>b</sup> Irina Dvorkin<sup>c</sup>

<sup>a</sup>Astrophysics, University of Oxford, DWB, Keble Road, Oxford, OX1 3RH, UK

<sup>b</sup>Université de Genève, Département de Physique Théorique and Centre for Astroparticle Physics, 24 quai Ernest-Ansermet, CH-1211 Genève 4, Switzerland

<sup>c</sup>Sorbonne Université, CNRS, UMR 7095, Institut d'Astrophysique de Paris, 98 bis boulevard Arago, 75014 Paris, France

E-mail: [giulia.cusin@physics.ox.ac.uk](mailto:giulia.cusin@physics.ox.ac.uk), [ruth.durrer@unige.ch](mailto:ruth.durrer@unige.ch), [dvorkin@iap.fr](mailto:dvorkin@iap.fr)

**Abstract.** In this paper we study gravitational lensing of gravitational wave events. The main point of the present work is to introduce a semi-analytic approach so that each ingredient can be varied and tested individually. Our analytic model for the source population is motivated by a numerical study and we compare semi-analytical and numerical results. We determine the expected magnification for events seen at a given observed luminosity distance. We find that while the probability of significant magnification of the observed LIGO-Virgo events is very small, the probability distribution of the magnification has a significant tail to high  $\mu$  such that e.g. the variance of the magnification is very large and even diverges in the geometric optics approximation. For the 10 binary black hole mergers observed by LIGO-Virgo in the O1+O2 observation campaigns, the probability that one of them has been magnified with magnification of 5 or bigger is  $\mathcal{P}_{\text{obs}}(> 5) \sim 0.01$  while the probability of magnification by 50 or bigger is  $\mathcal{P}_{\text{obs}}(> 50) \sim 0.005$ .

---

## Contents

<b>1</b>	<b>Introduction</b>	<b>1</b>
<b>2</b>	<b>The theory</b>	<b>2</b>
2.1	Notation	2
2.2	A singular isothermal sphere model for lens	4
2.3	Cross section	5
2.4	Optical depth and lensing probability	5
2.5	Average amplification	6
2.6	Average time delay	10
<b>3</b>	<b>A simple model for semi-analytical results</b>	<b>10</b>
3.1	Analytic description of lenses: probability density	10
3.2	Analytic description of binary population: emission and distribution	11
3.3	Analytical results for the LIGO detector(s)	15
<b>4</b>	<b>Numerical results</b>	<b>17</b>
4.1	The lens distribution	17
4.2	Results for optical depth and probability	18
4.3	Modeling the distribution of GW sources	20
4.4	The average amplification	22
<b>5</b>	<b>Discussion and conclusion</b>	<b>24</b>
<b>A</b>	<b>Fit to the Illustris simulation</b>	<b>30</b>
<b>B</b>	<b>Analytic model: Amplification as function of the luminosity</b>	<b>30</b>

---

## 1 Introduction

The direct detection of gravitational waves from inspiraling binary black holes and neutron stars by the LIGO and Virgo experiments [1–8] has been one of the greatest successes in experimental physics and observational astronomy in recent years. Not only does it lead to unprecedented insights on black holes and especially neutron stars, but it also allows us to test general relativity (GR) and cosmology.

An interesting aspect is the fact that the clustered matter between the gravitational wave source and the observer can amplify the observed signal. This can lead to an underestimation of the comoving distance to the source and therefore of its redshift which in turn leads to an overestimation of the chirp mass [9]. It has even been proposed, that the masses of the black hole mergers observed by LIGO have been substantially overestimated due to this lensing effect [10].

In this paper, we want to determine the probability that an event of a given strain amplitude, or rather of a given signal to noise ratio (SNR) for fixed experiment characteristics, is being significantly magnified by lensing. We want to study the dependence of the strong lensing probability and of the mean magnification on redshift and on the strain amplitude (or SNR). Similar studies

are already present in the literature [9, 11–13]. The main difference to the present work is that instead of full numerical simulations, we present semi-analytic formulae which can be applied to an arbitrary lens and source distribution keeping full control of modelling and transparency of all physical effects. This allows us to study the dependence of the result on the lens and/or source distribution which otherwise is quite obscure. We model the lenses as singular isothermal sphere lenses which is not particularly realistic, but allows for analytic calculations of most quantities and is sufficient for statistical purposes.

The remainder of this paper is structured as follows: In the next section we derive the equations for the lensing probability, mean magnification and other quantities of interest. In section 3 we discuss a simple analytical model which is useful to understand the physics. In section 4 we introduce a numerical study for the population of lenses and sources and we present numerical results for the magnification as a function of both real and observed redshift, for the LIGO-Virgo detector network. In section 5 we discuss our results and conclude. Some details are deferred to an appendix.

## 2 The theory

In this section we present our theoretical model: we describe galaxies acting as lenses as singular isothermal spheres (SIS) and we derive expressions for the magnification and time delay between multiple images as a function of the geometrical quantities entering the picture. SIS are not a very realistic lens model but since we are interested in statistical averages and not in the detailed modelling of a single lens, the fact that individual lenses will in general be triaxial and have substructure is expected to average out.

### 2.1 Notation

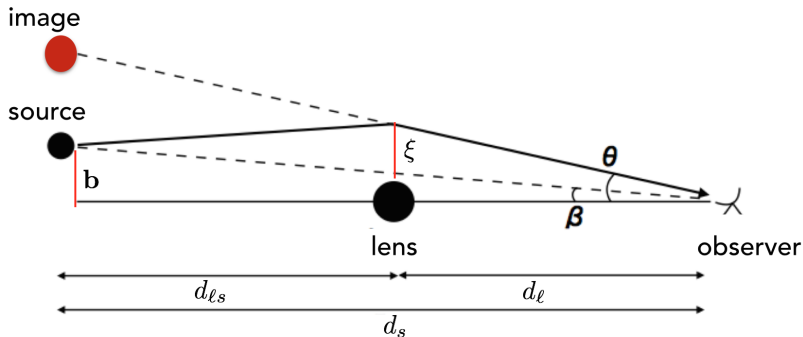


**Figure 1.** A gravitational lens.

In this paper we set  $c = 1$  but keep the gravitational constant  $G$ . Let us first fix the notation. In Fig. 1 we schematically illustrate a lens. We define  $\theta$  and  $\beta$  as the lensed and the unlensed angular position of the source. The optical axis is connecting the observer to the center of mass of the lens. We introduce a vector in the source plane from the optical axis to the source,  $\mathbf{b} = d_s \boldsymbol{\beta}$  and a vector  $\boldsymbol{\xi}$  in the lens plane defined as  $\boldsymbol{\xi} = \theta d_{\ell}$ . This fixes the geometry. Here  $d_{\ell} = d(z_{\ell})$ ,  $d_{\ell s} = d(z_{\ell}, z_s)$  and  $d_s = d(z_s)$  are the angular diameter distances from the

observer to the lens, from the lens to the source and from the observer to the source respectively. The angular diameter distances in a spatially flat Friedman universe are

$$d_\ell = d(z_\ell) = \frac{1}{1+z_\ell} \chi(0, z_\ell), \quad (2.1)$$

$$d_{\ell s} = d(z_\ell, z_s) = \frac{1}{1+z_s} \chi(z_\ell, z_s), \quad (2.2)$$

$$d_s = d(z_s) = \frac{1}{1+z_s} \chi(0, z_s) = \frac{1+z_\ell}{1+z_s} d_\ell + d_s \quad \text{and} \quad (2.3)$$

$$\chi(z_1, z_2) = \int_{z_1}^{z_2} \frac{dz}{H(z)} = \chi(z_2) - \chi(z_1), \quad \left( \chi(0, z) \equiv \chi(z) \right) \quad (2.4)$$

is the comoving distance from redshift  $z_1$  to  $z_2$ . Here we assume vanishing spatial curvature and the present scale factor,  $a_0 = 1$ .

The lens equation is

$$\boldsymbol{\beta} = \boldsymbol{\theta} - \boldsymbol{\alpha}(\boldsymbol{\theta}), \quad (2.5)$$

where  $\boldsymbol{\alpha}$  is the deflection angle. We consider an axi-symmetric lens with dimensionless surface density

$$\kappa(\boldsymbol{\theta}) = \frac{\Sigma(|\boldsymbol{\theta}|)}{\Sigma_c}, \quad \theta = |\boldsymbol{\theta}|, \quad (2.6)$$

where we will define the critical surface density,  $\Sigma_c$ , conveniently such that  $\kappa$  becomes the convergence. Here  $\boldsymbol{\theta}$  is a 2-dim angle or a dimensionless variable on the surface normal to the line of sight, and the surface density is given in terms of the mass density  $\rho$  as

$$\Sigma(\boldsymbol{\theta}) = \int_{-\infty}^{\infty} d\ell \rho(\ell, d_\ell \boldsymbol{\theta}). \quad (2.7)$$

Axi-symmetry implies that  $\Sigma$  depends only on  $\theta = |\boldsymbol{\theta}|$  and  $d_\ell$  is the angular diameter distance to the center of the lens. The 2-dimensional deflection angle is then given by

$$\boldsymbol{\alpha}(\boldsymbol{\theta}) = \frac{1}{\pi} \int d^2 \theta' \frac{\boldsymbol{\theta} - \boldsymbol{\theta}'}{|\boldsymbol{\theta} - \boldsymbol{\theta}'|^2} \kappa(\theta'). \quad (2.8)$$

Integration yields

$$\boldsymbol{\alpha}(\boldsymbol{\theta}) = \frac{\boldsymbol{\theta}}{\theta} \alpha(\theta), \quad \alpha(\theta) = \frac{2}{\theta} \int_0^\theta d\theta' \theta' \kappa(\theta'). \quad (2.9)$$

The time delay between two images seen at positions  $\boldsymbol{\theta}^{(1)}$  and  $\boldsymbol{\theta}^{(2)}$  is given by

$$\Delta t = t_1 - t_2 = (1+z_\ell) \frac{d_s d_\ell}{d_{\ell s}} \left[ \Phi(\boldsymbol{\theta}^{(1)}, \boldsymbol{\beta}) - \Phi(\boldsymbol{\theta}^{(2)}, \boldsymbol{\beta}) \right], \quad (2.10)$$

where the Fermat potential  $\Phi$  is

$$\Phi(\boldsymbol{\theta}, \boldsymbol{\beta}) = \frac{1}{2} (\boldsymbol{\theta} - \boldsymbol{\beta})^2 - \psi(\boldsymbol{\theta}), \quad (2.11)$$

and  $\psi(\boldsymbol{\theta})$  is the (dimensionless) lensing potential given by

$$\psi(\boldsymbol{\theta}) = \int d^2 \theta' \kappa(\theta') \log \left( \frac{|\boldsymbol{\theta} - \boldsymbol{\theta}'|}{\theta_0} \right) + \text{const.}, \quad (2.12)$$

defined such that  $\boldsymbol{\alpha} = \nabla\psi$ .

In the axi-symmetric case, the lens equation reduces to the scalar equation

$$\beta = \theta - \alpha(\theta). \quad (2.13)$$

In the limit  $\beta \rightarrow 0$  the lensed image forms a ring with radius  $\theta_E$ , solution of

$$\theta_E - \alpha(\theta_E) = 0. \quad (2.14)$$

## 2.2 A singular isothermal sphere model for lens

The matter density of a *singular isothermal sphere* is given by

$$\rho(r) = \frac{\sigma_v^2}{2\pi G r^2}, \quad (2.15)$$

where  $\sigma_v^2$  denotes the velocity dispersion of the lens. Despite its singularity in the center and infinite total mass, this can be considered as a rather realistic mass distribution for lensing by a galaxy (see [12, 14]);  $\sigma_v$  is the velocity dispersion inside the galaxy. Integrating along the line of sight we obtain

$$\Sigma(\theta) = \frac{\sigma_v^2}{2G} \frac{1}{d_\ell \theta}. \quad (2.16)$$

We set  $\Sigma_c = (4\pi G)^{-1} d_s / (d_{\ell s} d_\ell)$  so that

$$\kappa(\theta) = 2\pi \sigma_v^2 \frac{d_{\ell s}}{d_s} \frac{1}{\theta}. \quad (2.17)$$

Inserting  $\kappa$  in (2.9) we obtain

$$\alpha(\theta) = 4\pi \sigma_v^2 \frac{d_{\ell s}}{d_s} \equiv \alpha_0. \quad (2.18)$$

We now rescale our variables by  $\alpha_0$ , introducing

$$\mathbf{x} = \frac{\boldsymbol{\theta}}{\alpha_0} \quad \text{rescaled image position}, \quad (2.19)$$

$$\mathbf{a} = \frac{\boldsymbol{\alpha}}{\alpha_0} \quad \text{rescaled deflection angle}, \quad (2.20)$$

$$\mathbf{y} = \mathbf{x} - \mathbf{a} \quad \text{rescaled source position}. \quad (2.21)$$

In terms of these rescaled variables, the lens equation for the SIS simply becomes

$$\mathbf{y} = \mathbf{x} - \frac{\mathbf{x}}{|\mathbf{x}|}. \quad (2.22)$$

For  $\mathbf{y} = 0$  the solution is the Einstein ring  $|\mathbf{x}| = 1$ , for  $y = |\mathbf{y}| < 1$  there are two solutions. One with  $x_1 = |\mathbf{x}_1| = 1 + y$  on the same side of the line of sight as the source (positive parity) and one with  $x_2 = |\mathbf{x}_2| = 1 - y$  on the opposite side (negative parity). For  $y > 1$  the second solution no longer exists. The Jacobian of the lens map is

$$A_{ij} = \delta_{ij} \left( 1 - \frac{1}{|\mathbf{x}|} \right) + \frac{x_i x_j}{|\mathbf{x}|^3}, \quad \det A = 1 - \frac{1}{|\mathbf{x}|}, \quad \mu = \frac{1}{|\det A|} = \frac{|\mathbf{x}|}{|1 - |\mathbf{x}||}, \quad (2.23)$$

where we have introduced the magnification  $\mu$ . Expressing the total magnification of a point source at position  $y$  in terms of  $y$  we find

$$\mu(y) = \begin{cases} \mu(\mathbf{x}_1) + \mu(\mathbf{x}_2) = \frac{y+1}{y} + \frac{1-y}{y} = \mu_1 + \mu_2 = \frac{2}{y}, & y \leq 1, \\ \frac{y+1}{y} = 1 + \frac{1}{y}, & y \geq 1. \end{cases} \quad (2.24)$$

The lensing potential is simply  $\psi(x) = |x|$  and the time delay between the two images is

$$\Delta t = [4\pi\sigma_v^2]^2 \frac{d_\ell d_{\ell s}}{d_s} (1 + z_\ell) 2y = \beta(\sigma_v^2, z_\ell, z_s) y, \quad (2.25)$$

where  $2y = x_1 - x_2$ .

### 2.3 Cross section

The impact parameter of the source (in the source plane) is given by  $|\mathbf{b}| = b = y\alpha_0 d_s$ . A source with impact parameter smaller or equal to  $b$  is amplified by at least a factor  $\mu(y)$ . Hence the cross section for amplification by a factor more than  $\mu_1$  of the stronger image from an SIS lens with velocity dispersion  $\sigma_v$  is

$$\sigma(\mu_1, z_\ell, z_s, \sigma_v) = \pi b^2 = \pi(y\alpha_0 d_s)^2 = \frac{\pi(4\pi)^2 \sigma_v^4 d_{\ell s}^2}{(\mu_1 - 1)^2}. \quad (2.26)$$

This result remains correct also for  $y \geq 1$ , where we have only one image with magnification  $\mu_1$  which tends to 1 when  $y \rightarrow \infty$ .

It is important that in the case of gravitational wave events we consider only one image and not the sum of both, since we expect to see a short burst of GWs which comes only from one image. The second image is delayed in time. Since we are interested in magnification, we shall compute the cross section for the stronger image. This point has been neglected in the previous literature where in (2.26)  $y^{-1} = \mu_1 - 1$  is replaced by  $y^{-1} = \mu/2 = (\mu_1 + \mu_2)/2$  which is the correct expression for a static situation where both images are seen together. For strong amplification,  $\mu_1 \sim \mu_2 \gg 1$  the difference reduces the cross section by a factor 4.

For  $y < 1$ , i.e. in the situation where we have two images, we can rewrite eq. (2.26) also in terms of the time delay between the two images, using the relation (2.25). Explicitly one obtains

$$\sigma(\Delta t, z_\ell, z_s, \sigma_v) = \frac{1}{64\pi} \left(\frac{d_s}{d_\ell}\right)^2 \sigma_v^{-4} \frac{1}{(1 + z_\ell)^2} \Delta t^2. \quad (2.27)$$

### 2.4 Optical depth and lensing probability

To compute the optical depth to the source,  $\tau(\mu, z_s)$  we need to know the density  $n(\sigma_v, z_\ell)$  of lenses (galaxies) with a given velocity dispersion  $\sigma_v$  at redshift  $z_\ell$ . We define the density  $n(\sigma_v, z_\ell)$  such that its integral  $\int n(\sigma_v, z_\ell) d\sigma_v$  simply gives the total density of lenses at redshift  $z_\ell$ . Then (do not mixup the cross section,  $\sigma$  and the velocity dispersion,  $\sigma_v$ )

$$\int \sigma(\mu, z_\ell, z_s, \sigma_v) n(\sigma_v, z_\ell) d\sigma_v, \quad (2.28)$$

is the rate of scatterings leading to a magnification larger than  $\mu$  and

$$\tau(\mu, z_s) = \int_0^{z_s} dz_\ell \frac{dr}{dz_\ell} \int \sigma(\mu, z_\ell, z_s, \sigma_v) n(\sigma_v, z_\ell) d\sigma_v, \quad (2.29)$$

is the optical depth to lensing with magnification  $\geq \mu$  (of the more strongly magnified image in the case of two images) for a source at redshift  $z_s$ . Here  $dr$  is the physical length element at redshift  $z_\ell$ ,

$$\frac{dr}{dz_\ell} = \frac{1}{(1+z_\ell)H(z_\ell)}. \quad (2.30)$$

Inserting our expressions we obtain

$$\tau(\mu, z_s) = \frac{\pi(4\pi)^2}{(\mu-1)^2(1+z_s)^2} \int_0^{z_s} dz \frac{\chi^2(z, z_s)}{(1+z)H(z)} \int_0^\infty d\sigma_v \sigma_v^4 n(\sigma_v, z). \quad (2.31)$$

Often only the strong lensing case is considered and the magnification from the two images is added to give the total magnification. To do this one has to replace  $1/(\mu-1)^2$  by  $4/\mu^2$ . As already mentioned above, here we cannot do this since in the case of strong magnification and double images we expect a considerable time delay, so that typically we observe only one image at one given time. Here we assume this to be the stronger image. In the strong magnification case,  $\mu \gg 2$ , this difference is roughly a factor 4, while in the limit  $y \rightarrow 1$  where  $\mu \rightarrow 2$  and the second image disappears, the two expressions agree.

The probability of having an event from redshift  $z_s$  magnified more than  $\mu$  is

$$P(> \mu, z_s) = 1 - \exp(-\tau(\mu, z_s)) = \int_\mu^\infty p(\mu, z_s) d\mu, \quad (2.32)$$

where  $p(\mu, z_s)$  is the probability density for magnification by  $\mu$ ,

$$p(\mu, z_s) = -\frac{d}{d\mu} P(> \mu, z_s) = -\frac{d\tau}{d\mu} \exp(-\tau(\mu, z_s)). \quad (2.33)$$

We can repeat similar steps to compute the probability that a source is strongly lensed and two images are produced with a time separation  $\Delta t$ . The optical depth is given by

$$\tau(\Delta t, z_s) = \int_0^{z_s} \frac{dz_\ell}{(1+z_\ell)H(z_\ell)} \int \Theta(1/2 - y) \sigma(\Delta t, z_\ell, z_s, \sigma_v) n(\sigma_v, z_\ell) d\sigma_v, \quad (2.34)$$

where the Heaviside function,  $\Theta$ , has been introduced in order to request that the luminosity of the weaker image is not less than 1/3 that of the stronger image. Replacing the factor 1/3 by some arbitrary factor  $f$  corresponds to replacing the bound 1/2 in the Heaviside function by  $(1-f)/(1+f)$ . Note that here  $y(z_s, z_\ell, \Delta t, \sigma_v)$  has to be considered as function of the lens and source redshift for fixed  $\Delta t$  as given in eq. (2.25). We can also compute the probability density for a time delay of  $\Delta t$  as

$$p(\Delta t, z_s) = -\frac{d\tau}{d\Delta t} \exp(-\tau(\Delta t, z_s)). \quad (2.35)$$

## 2.5 Average amplification

We now determine the average amplification expected for a given distribution of sources. Here  $d\mathcal{N}(L, z_s) = N(L, z_s) dL dz_s$  denotes number of sources at redshift  $z_s$  with luminosity  $L$  in a bin of width  $dz_s$  and  $dL$  in redshifts and intensity space. Note that even though the wording here is very much borrowed from optical astronomy, in a fixed frequency band, the *luminosity* is simply

proportional to the square of the strain and hence can be replaced by the strain as we shall do below. Without magnification the flux of such a source on Earth is

$$F(L, z_s) = \frac{L}{4\pi((1+z_s)\chi(z_s))^2}, \quad L(F, z_s) = 4\pi((1+z_s)\chi(z_s))^2 F. \quad (2.36)$$

A realistic GW detector has a limiting strain sensitivity, usually cast as an SNR limit,  $\rho_{\text{lim}}$ . A source is detected if  $\rho \geq \rho_{\text{lim}}$ , where the SNR  $\rho$  is defined by [15]

$$\rho^2 = 4 \int \frac{|h(f)|^2}{S_n(f)} df = \int \rho^2(f) df. \quad (2.37)$$

Here  $S_n(f)$  is the noise of the detector at frequency  $f$  (see [16] for more details). We want to translate a limiting SNR  $\rho_{\text{lim}}$  into a limiting flux,  $F_{\text{lim}}$ . The flux per frequency band,  $F(f)$  is related to the energy density per frequency band,  $\epsilon(f)$ , of the gravitational wave by

$$F(f) = c\epsilon(f) = \frac{(2\pi)^2 c}{16\pi G} f^2 |h(f)|^2 = \frac{\pi}{16G} f^2 S_n(f) \rho^2(f), \quad (2.38)$$

where we have set the speed of light,  $c \equiv 1$  for the last equal sign, as in the rest of this paper. At fixed noise level and in a small frequency band, therefore  $F_{\text{lim}} \propto \rho_{\text{lim}}^2$ . For fixed source luminosity, the limiting flux scales like  $F_{\text{lim}} \propto \mu$ , hence  $\rho_{\text{lim}} \propto \sqrt{\mu}$ .

A flux limit defines a region in the plane  $(L, D(z_s))$  defined by  $F(L, D(z_s)) > F_{\text{lim}}$ , where  $D_s \equiv D(z_s) = (1+z_s)\chi(z_s) = (1+z_s)^2 d_s$  denotes the luminosity distance of the source. Given a source distribution  $N(L, z_s)$ , the number of sources which we detect in a redshift bin of size  $dz_s$  around redshift  $z_s$  without considering amplification is

$$d\mathcal{N}(F_{\text{lim}}, z_s) = dz_s \int_{L(F_{\text{lim}}, z_s)}^{\infty} N(L, z_s) dL. \quad (2.39)$$

Equivalently, the number of sources that we can detect with an emitted luminosity  $L \pm dL/2$  is

$$d\mathcal{N}(F_{\text{lim}}, L) = dL \int_0^{D_s(F_{\text{lim}}, L)} N(L, z_s) \frac{dz_s}{dD_s} dD_s, \quad (2.40)$$

where  $D_s(F_{\text{lim}}, L)$  is defined by

$$F(L, D_s(F_{\text{lim}}, L)) = F_{\text{lim}}.$$

If an event is magnified by  $\mu > 1$  we see it even if without magnification its flux would have been  $F_{\text{lim}}/\mu$ , hence the lower limit of the integral (2.39) can be correspondingly reduced. The total number of objects which we see from redshift  $z_s \pm dz_s/2$  including magnification is

$$d\mathcal{N}_{\text{obs}}(z_s, F_{\text{lim}}) = dz_s \int_1^{\infty} d\mu p(\mu, z_s) \int_{L_{\text{lim}}(z_s)/\mu}^{\infty} N(L, z_s) dL, \quad (2.41)$$

where  $L_{\text{lim}}(z_s) = L(F_{\text{lim}}, z_s)$ . The quantity which is integrated over  $\mu$  is actually the number of sources which need to be amplified by a factor of at most  $\mu$  so as to be seen from a redshift bin  $dz_s$  around  $z_s$ . For future use, we define this quantity as

$$d\mathcal{N}(\mu, z_s) \equiv dz_s \int_{L_{\text{lim}}(z_s)/\mu}^{\infty} N(L, z_s) dL. \quad (2.42)$$



Correspondingly, the mean amplification is

$$\langle \mu \rangle(z_s) = \frac{\int_1^\infty d\mu \mu p(\mu, z_s) d\mathcal{N}(\mu, z_s)}{\int_1^\infty d\mu p(\mu, z_s) d\mathcal{N}(\mu, z_s)}, \quad (2.43)$$

which of course depends on the threshold in flux  $F_{\text{lim}}$ , i.e. on the detector sensitivity. Note that (2.43) is the first moment of the probability distribution

$$\mathcal{P}_z(\mu) \equiv \mathcal{C} p(\mu, z) d\mathcal{N}(\mu, z), \quad (2.44)$$

where  $\mathcal{C}$  is a normalization constant. For sufficiently high  $\mu$ ,  $p(\mu, z) \simeq -d\tau/d\mu \propto \mu^{-3}$ , while the number of sources with amplification  $\mu$ , eq. (2.42), becomes independent of  $\mu$  for large values of  $\mu$  (we simply see all sources).<sup>1</sup> Then the integral of (2.42),  $\mathcal{P}_z(> \mu) \propto \mu^{-2}$  and the variance of the distribution, defined by  $\text{Var}(\mu) \equiv \langle \mu^2 \rangle - \langle \mu \rangle^2$  is log-divergent. We stress that this is a general property of the probability distribution of magnification in strong lensing. It does not depend on the details of the distribution of sources, nor on the details of the lens distribution. Moreover, it applies also to the case of transient electromagnetic sources lensed by galaxies: the first moment of the magnification (the mean) is well defined, but the variance is log-divergent. Of course this divergence is not physical. When the magnification becomes very large,  $y$  is very small and the geometric optics treatment adopted here breaks down. Nevertheless, this indicates that the distribution has a significant tail with large magnification. Even though, as we shall see, the probability for a magnification of e.g. 10 is very small, it is not exponentially small as for a Gaussian distribution but it only decays as a mild power law.

The functions determined here, however are not truly relevant as we typically do not know the (true) redshift of a GW event. We usually infer it by assuming that the observed luminosity distance is the one of the background universe without magnification. This is of course not true when the magnification is substantial. We therefore rewrite (2.41) and (2.43) as a functions of the observed luminosity distance which is extracted from observations. This is given by

$$D_{\text{obs}} \equiv \frac{D_s}{\sqrt{\mu}}. \quad (2.45)$$

In eq. (2.43) we rewrite  $p(\mu, z_s) = p(\mu, z_s(D_{\text{obs}}, \mu))$ , i.e. as the probability that a source that appears at a distance  $D_{\text{obs}}$  has been amplified of  $\mu$ . Analogously,  $dN(L, z_s) = dN(L, z_s(D_{\text{obs}}, \mu))$  is the number of sources emitting luminosity  $L$ , and which appear at a luminosity distance  $D_{\text{obs}}$  associated to redshift  $z_s$  and magnification  $\mu$  through (2.45), per unit redshift and intensity. The number of sources seen from an observed luminosity distance  $D_{\text{obs}}$  is<sup>2</sup>

$$\begin{aligned} dN_{\text{obs}}(D_{\text{obs}}, F_{\text{lim}}) &= dD_{\text{obs}} \int dN_{\text{obs}}(z_s, F_{\text{lim}}) \delta\left(\frac{D_s(z_s)}{\sqrt{\mu}} - D_{\text{obs}}\right) \\ &= dD_{\text{obs}} \int_1^\infty d\mu p(\mu, z_s(D_{\text{obs}}, \mu)) \frac{\sqrt{\mu}}{D'_s(z_s(D_{\text{obs}}, \mu))} \int_{L_{\text{lim}}/\mu}^\infty N(L, z_s(D_{\text{obs}}, \mu)) dL, \end{aligned} \quad (2.46)$$

where

$$D'_s(z) \equiv \frac{dD_s}{dz} = \chi(z) + \frac{1+z}{H(z)}. \quad (2.47)$$

<sup>1</sup>This last statement is general and does not depend on the details of the distribution of sources. It follows from the physical assumption that there exist a minimum value for the intrinsic luminosity emitted,  $L_{\text{min}}$ , and once  $\mu$  is such that  $L_{\text{lim}}/\mu < L_{\text{min}}$  we see all sources and the luminosity integral no longer depends on  $\mu$ .

<sup>2</sup>Note that now the factor  $dz_s$  has to be replaced by  $(dD_{\text{obs}}/dz_s)^{-1} dD_{\text{obs}} = \sqrt{\mu} (dD_s/dz_s)^{-1} dD_{\text{obs}}$ .

For later use, we also introduce  $z_{\text{obs}}$  defined by  $D_s(z_{\text{obs}}) = D_{\text{obs}}$ , i.e. the redshift inferred by an observer who assumes that  $D_{\text{obs}}$  is the luminosity distance of the background universe (without magnification). The quantity in (2.46) is the number density of sources that we see at a luminosity distance  $D_{\text{obs}}$ . For future use, we define the number of objects seen from a luminosity distance  $D_{\text{obs}} \pm dD_{\text{obs}}/2$  and with magnification  $\mu$  as

$$d\mathcal{N}(\mu, D_{\text{obs}}) \equiv dD_{\text{obs}} \frac{\sqrt{\mu}}{D'_s(z_s(D_{\text{obs}}, \mu))} \int_{L_{\text{lim}}}^{\infty} N(L, z_s(D_{\text{obs}}, \mu)) dL, \quad (2.48)$$

where it is understood that  $L_{\text{lim}} \equiv L(F_{\text{lim}}, D_{\text{obs}}) = 4\pi D_{\text{obs}}^2 F_{\text{lim}}$ . The convolution of this quantity (2.48) with the probability density of magnification gives the total number of events observed from a given observed luminosity, eq. (2.46). The average amplification as a function of the observed luminosity distance is therefore

$$\langle \mu \rangle(D_{\text{obs}}) = \frac{\int_1^{\infty} d\mu \mu p(\mu, D_{\text{obs}}) d\mathcal{N}(\mu, D_{\text{obs}})}{\int_1^{\infty} d\mu p(\mu, D_{\text{obs}}) d\mathcal{N}(\mu, D_{\text{obs}})}, \quad (2.49)$$

which of course depends on the threshold in flux  $F_{\text{lim}}$ , i.e. on the detector sensitivity. In full analogy with eq. (2.44), we can introduce the probability distribution of magnification (for different observed luminosity distance of the source)

$$\mathcal{P}_{\text{obs}}(\mu) \equiv \mathcal{C} p(\mu, D_{\text{obs}}) d\mathcal{N}(\mu, D_{\text{obs}}), \quad (2.50)$$

where  $\mathcal{C}$  is a constant of normalization. From eq. (2.48), it follows that  $d\mathcal{N}(\mu, D_{\text{obs}}) \propto \sqrt{\mu}$  for  $\mu \gg 1$ . The probability density  $p(\mu, D_{\text{obs}})$  in (2.50) depends on  $\mu$  also through the observed luminosity as we have defined  $p(\mu, D_{\text{obs}}) \equiv p(\mu, z_s(\sqrt{\mu}D_{\text{obs}}))$ . Recalling that  $p(\mu, z_s) \propto \mu^{-3}$ , it follows that  $p(\mu, D_{\text{obs}})$  will have a milder decay with magnification.<sup>3</sup> The exact scaling of  $p(\mu, D_{\text{obs}})$  with  $\mu$  depends on the details of the lens distribution. For a realistic distribution with comoving number density of lenses which reproduces observation (or hydrodynamical simulation calibrated to observations), we find that  $p(\mu, D_{\text{obs}}) \propto \mu^{-\alpha}$ . The value of  $\alpha$  increases from 2.2 to 3 as we move the observed luminosity distance from  $\sim 300\text{Mpc}$  to  $1500\text{Mpc}$  where it saturates to the asymptotic value  $\alpha = 3$ . It follows that the probability distribution (2.50) scales as  $\mathcal{P}_{\text{obs}}(\mu) \propto \mu^{-\alpha+1/2}$  and its integral from  $\mu$  to infinity behaves as  $\mathcal{P}_{\text{obs}}(> \mu) \propto \mu^{-\alpha+3/2}$  for large values of  $\mu$ . It follows that, for any fixed value of  $D_{\text{obs}}$  the variance of the distribution diverges as  $\mu^{-\alpha+7/2}$ . We stress that this is a general property of the probability distribution of magnification (for different observed redshift), independent on the details of the distribution of sources. Moreover, it applies also to the case of strongly lensed sources of electromagnetic radiation. Also in that case, the variance of the distribution of magnification (for different observed redshift) is divergent. We observe that for realistic models of lens distribution also the mean of (2.50) diverges for small observed distances. We will get back to this point in Sec. 4 and 5.<sup>4</sup>

<sup>3</sup>Indeed, for a fixed  $D = D_{\text{obs}}$ , and  $\mu > 1$ ,  $p(\mu, D_{\text{obs}}) \equiv p(\mu, z_s(\sqrt{\mu}D_{\text{obs}}))$  comes from a redshift which is higher than  $z_s(D)$  and therefore the lensing probability is higher.

<sup>4</sup>The fact that the variance of the distribution diverges is due to the presence of extremely highly magnified sources, i.e. sources aligned along the lens-observer direction for which the magnification  $\mu \rightarrow \infty$ , see eq. (2.24). This is also at the origin of the divergence of the mean of the magnification at small observed distances. Physically, the magnification tends to a finite value and, as mentioned above, the presence of the divergence is due to the geometric optics approximation, which breaks down in the vicinity of caustics, where wave effects need to be taken into account. The fact that the mean of the magnification diverges only for small observed distances is due to the fact that, if a given source is very highly magnified, it appears at a small distance.

## 2.6 Average time delay

The average time delay can not be obtained in a corresponding way. The problem is that both,  $z_s(D_{\text{obs}}, \mu)$  and the lower bound of the intensity integral depend on the magnification, while the probability density  $p(\Delta t, z_s)$  has contributions from different magnifications. On the other hand, a fixed magnification  $\mu$  can lead to different time delays depending on the velocity dispersion  $\sigma_v$  of the lensing galaxy and on its redshift,  $z_\ell$ . However, in order to have a double image which can lead to time delay, the magnification of the stronger image is  $\mu_1 = 1 + 1/y > 2$  since  $y < 1$  is required.

It is convenient in this case to explicitly keep the dependence on  $(z_\ell, z_s, \sigma_v, \Delta t)$  and integrate over these only at the very end when computing the average  $\Delta t$ . We then have for the optical depth

$$\tau(\Delta t, z_s, z_\ell, \sigma_v) = \frac{1}{(1 + z_\ell)H(z_\ell)} \sigma(\Delta t, z_\ell, z_s, \sigma_v) n(\sigma_v, z_\ell). \quad (2.51)$$

We can compute the probability density as

$$p(\Delta t, z_s, z_\ell, \sigma_v) = -\frac{d\tau}{d\Delta t} \exp(-\tau(\Delta t, z_s, z_\ell, \sigma_v)). \quad (2.52)$$

The average time delay for a source observed at luminosity distance  $D_{\text{obs}}$  is given by

$$\langle \Delta t \rangle (D_{\text{obs}}) = \frac{\int_0^\infty d\Delta t \int dz_\ell \int d\sigma_v \Delta t p(\Delta t, D_{\text{obs}}, z_\ell, \sigma_v) (dz_s/dD_{\text{obs}}) \int_{L_{\text{lim}}/\mu_2}^\infty N(L, D_{\text{obs}}) dL}{\mathcal{N}_{\text{obs}}(D_{\text{obs}}, F_{\text{lim}})}, \quad (2.53)$$

where we are considering the magnification of the fainter image giving the lowest integration bound over intensity to make sure that both images are seen

$$\mu_2(\Delta t, D_{\text{obs}}, z_\ell, \sigma_v) = \frac{\beta(\sigma_v^2, z_\ell, z_s)}{\Delta t} - 1. \quad (2.54)$$

## 3 A simple model for semi-analytical results

Let us first discuss a simplified analytical model to have some indication for the mean magnification as a function of redshift. The advantage of an analytic description is that it allows us to analyze the dependence of the results on the various astrophysical ingredients entering the modelling. We need two basic ingredients: a model for the lens distribution in order to derive the probability density of lensing, and a model for the distribution of sources as a function of redshift and intensity.

### 3.1 Analytic description of lenses: probability density

If there would be no evolution of lenses we would expect the physical number density of galaxies to scale with redshift as  $n(\sigma_v, z) \propto (1 + z)^3$ . Let us now assume that in the considered redshift range a lot of galaxies are forming such that

$$\int_0^\infty d\sigma_v \sigma_v^4 n(\sigma_v, z) = (1 + z) N \langle \sigma_v^4 \rangle, \quad (3.1)$$

where  $N$  is a galaxy density and  $\langle \sigma_v^4 \rangle$  a mean of the velocity dispersion to power 4. We postulate this law of evolution not because it is very realistic, but because it allows us to integrate the optical depth analytically. As we shall see, evolution is actually somewhat slower, but this seems not to

affect the result very significantly. With this, the factor  $1/(1+z)$  in (2.31) cancels and using  $\chi(z, z_s)' = -H(z)^{-1}$  we obtain

$$\tau(\mu, z_s) = \frac{\pi(4\pi)^2 \langle \sigma_v^4 \rangle N}{(\mu-1)^2 (1+z_s)^2} \int_0^{\chi(0, z_s)} d\chi \chi^2 = \frac{\pi(4\pi)^2 \langle \sigma_v^4 \rangle N \chi_s^3}{3(\mu-1)^2 (1+z_s)^2}. \quad (3.2)$$

We shall study a more realistic case in the next section. Crude estimates for  $N$  and  $\sigma_v$  are

$$N = 10^{10} H_0^3, \quad \langle \sigma_v^4 \rangle = (150 \text{ km/s})^4 \simeq 5 \times 10^{-14}. \quad (3.3)$$

With this we have for the optical depth

$$\tau(\mu, z_s) \simeq \frac{0.1}{(\mu-1)^2} \frac{(H_0 \chi(z_s))^3}{(1+z_s)^2}. \quad (3.4)$$

In Figs. 2 and 3 we show the optical depth in this simplified model for various values of magnification. The fact that  $\tau$  decays again after  $z \sim 2$  comes from the decrease of the lensing cross section  $\sigma \propto D_{\ell_s}^2 \propto (1+z_s)^{-2}$  with redshift. The higher number of lenses for sources at higher redshift can no longer compensate this for the redshift dependence which we have chosen here. For our simple model we find for the probability density

$$p(\mu, z_s) = \frac{2p_1(z_s)}{(\mu-1)^3} \exp\left(-\frac{p_1(z_s)}{(\mu-1)^2}\right), \quad \text{where} \quad p_1(z_s) = 0.1 \frac{(H_0 \chi(z_s))^3}{(1+z_s)^2}. \quad (3.5)$$

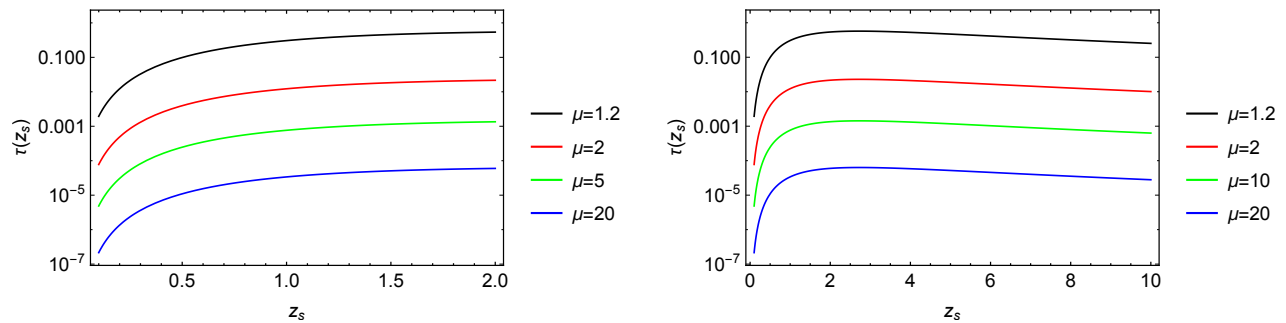


**Figure 2.** The optical depth,  $\tau(\mu, z)$ , as a function of redshift for different values of  $\mu = 1.2, 2, 5, 20$  from top to bottom. (Left:  $0 < z_s < 2$ . Right:  $0 < z_s < 10$ .) We have also compared our results with the numerical ones of [13] and up to the redshift considered in this reference,  $z = 5$ , they agree surprisingly well.

### 3.2 Analytic description of binary population: emission and distribution

In this section we work out an analytic model to describe the number density of sources as a function of the emitted strain (or the SNR for a given detector configuration) and as a function of redshift. As a first step we review the derivation of the SNR of a binary system of compact objects at fixed redshift as a function of the component masses and of the noise power spectral density of the instrument(s). We introduce the SNR  $\rho$  for events merging at redshift  $z_s$  and observed in a frequency band around  $f$  as [15]

$$\rho^2(f, z_s) = 4 \frac{|h(f, z_s)|^2}{S_n(f)} \propto \frac{F(f, z_s)}{S_n(f)} = \frac{L(f, z_s)}{4\pi D(z_s)^2 S_n(f)}, \quad (3.6)$$

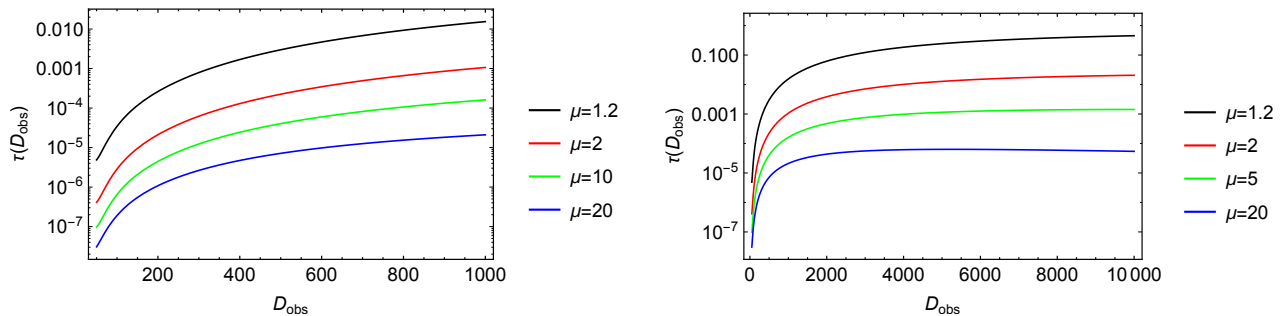


**Figure 3.** Optical depth as a function of the observed luminosity distance for different values of  $\mu = 1.2, 2, 5, 20$  from top to bottom.

where  $S_n(f)$  is the noise power spectrum of a given detector network, with dimension of  $\text{Hz}^{-1}$ . The SNR in a given frequency band is simply the integral of eq. (3.6) over that band. In eq. (3.6) we have defined the received flux per unit of frequency as  $F(f, z_s)$  and the related luminosity per unit of (observed) frequency as  $L(f, z_s)$ . Hence there is a one to one mapping between flux and SNR or luminosity and SNR. For a single binary system the SNR from the inspiral phase integrated over observed frequency is given by, see [15] (neglecting the merger and ringdown phases and writing explicitly the quantities the signal to noise depends to)

$$\rho^2(z_s, m, \mathcal{M}) = \frac{5}{96\pi^{4/3}} \frac{\Theta^2}{D^2(z_s)} (GM_z)^{5/3} f_{7/3}(z_s, m), \quad (3.7)$$

where  $\mathcal{M}_z = \mathcal{M}(1 + z_s)$  is the redshifted chirp mass of the system and  $m = m_1 + m_2$  is the total mass and the integral over frequencies can be approximated by

$$f_{7/3}(z_s, m) \equiv \int_0^{f_{\text{ISCO}}/(1+z_s)} df \left[ f^{7/3} S_n(f) \right]^{-1}, \quad (3.8)$$

with dimension  $[f_{7/3}] = [\text{Hz}]^{-1/3}$  while  $\Theta^2$  (with  $0 \leq \Theta^2 \leq 16$ ) is a geometrical factor that depends on the inclination of the binary and on the antenna pattern of the detector. Averaging over all angles one finds  $\overline{\Theta^2} = 64/25$ . We do not need this explicit expression in what follows and the interested reader is referred to [15] for details. In eq. (3.8) the upper integration bound is given by the (redshifted) frequency corresponding to the innermost stable circular orbit (ISCO) of the system, i.e. the frequency at which we consider the inspiraling phase of the system to end in our approximation. It is given by [16]

$$f_{\text{ISCO}} = \frac{1}{6\sqrt{6}(2\pi)} \frac{c^3}{Gm} \simeq 2.2 \text{ kHz} \left( \frac{M_\odot}{m} \right), \quad (3.9)$$

where  $m$  is the total mass of the binary system. We rewrite the standard parametrization (3.7) in a way which will be useful for what follows,

$$\rho^2(z_s, \mathcal{M}, m) = 7.7 \cdot 10^{-39} \Theta^2 \left( \frac{\mathcal{M}}{M_\odot} \right)^{5/3} \left( \frac{\text{Mpc}}{D(z_s)} \right)^2 \frac{f_{7/3}(z_s, m)}{\text{Hz}^{-1/3}} (1 + z_s)^{5/3}. \quad (3.10)$$

Let us understand the redshift dependence: from eq. (3.8) we see that if  $f_{\text{ISCO}}/(1 + z_s) > f_{\text{max}}$  then  $f_{7/3}(z_s)$  does not depend on redshift. Here with  $f_{\text{max}}$  we denote the maximum frequency a

given detector is sensitive to, (i.e., the frequency above which the noise becomes very large) and it is fixed by the form of the spectral noise in eq. (3.8). This is determined by the condition

$$(1 + z_s) < \frac{f_{\text{ISCO}}}{f_{\text{max}}} \simeq \left( \frac{2.2 \text{ kHz}}{f_{\text{max}}} \right) \left( \frac{M_{\odot}}{m} \right). \quad (3.11)$$

If this condition is verified for a given source, then (3.8) is redshift independent.

From a comparison with numerical models for source formation and evolution (see section 4), we find that the maximum SNR that we receive from a given redshift  $z_s$  can be effectively written as

$$\rho_{\text{max}}(z_s) = \mathcal{A} \left( \frac{\mathcal{M}_{\text{max}}}{M_{\odot}} \right)^{5/6} \frac{\text{Mpc}}{D(z_s)} (1 + z_s)^{5/6} \bar{f}_{7/3}(z_s)^{1/2}, \quad (3.12)$$

and similarly for the minimum value

$$\rho_{\text{min}}(z_s) = \mathcal{A} \left( \frac{\mathcal{M}_{\text{min}}}{M_{\odot}} \right)^{5/6} \frac{\text{Mpc}}{D(z_s)} (1 + z_s)^{5/6} \bar{f}_{7/3}(z_s)^{1/2}, \quad (3.13)$$

where  $\bar{f}_{7/3}(z_s)^{1/2}$  is obtained using the average ISCO frequency, rescaled with redshift, as upper cutoff in the integral (3.8), i.e. the ISCO frequency for the average total mass  $m$ . We have introduced a constant  $\mathcal{A} = 1.4 \cdot 10^{-19}$  which corresponds to the square root of the numerical factor in eq. (3.10) multiplied by the square root of  $\bar{\Theta}^2 = 64/25$ . For redshifts that satisfy the condition (3.11), eqs. (3.13) and (3.12) scale with redshift simply as  $(1 + z_s)^{5/6}$ .

As a second step, we need a parametrization for the number of sources per unit of SNR as a function of SNR and of redshift. The number density of sources per unit of chirp mass (and as a function of redshift) is given by

$$N(z_s, \mathcal{M}_c) \propto \mathcal{R}(z_s, \mathcal{M}_c) \propto p(\mathcal{M}_c), \quad (3.14)$$

where  $\mathcal{R}$  is the merger rate for a binary system with chirp mass  $\mathcal{M}_c$  at redshift  $z_s$  which in turn is proportional to the distribution of chirp masses (with redshift-dependent pre factors). For simplicity we assume it to be polynomial,  $p(\mathcal{M}_c) \propto \mathcal{M}_c^{-\beta_M}$ . We need now to convert the number density (3.14) into a number density per unit of signal to noise. Neglecting the mass dependence of the ISCO frequency, as we did in (3.13) and (3.12), we can simply invert (3.10) and write

$$N(\rho, z_s) = N_{\rho}(z_s) \rho^{-\gamma}, \quad (3.15)$$

with  $\gamma = (6\beta_M - 1)/5$  and  $N_{\rho}(z_s)$  is some redshift dependent function. Similarly, using eq. (3.6) we can work out the scaling of the number density of sources per unit of luminosity

$$N(L, z_s) = N_L(z_s) \left( \frac{L}{L_*} \right)^{-\beta}, \quad (3.16)$$

with  $\beta = 3(\beta_M - 1)/5$  and  $L_*$  is some reference luminosity. For example, the distribution of masses of the astrophysical model discussed in Section 4 is such that the resulting distribution of chirp masses is (independent on redshift)  $p(\mathcal{M}_c) \propto \mathcal{M}_c^{-3.2}$ . Then  $N(\rho, z_s) \propto \rho^{-3.6}$ , which is the scaling of the curves in Fig. 13.<sup>5</sup>

---

<sup>5</sup>Note that when comparing these figures to the scaling derived here, one needs to keep in mind that  $dN/d\rho = \rho^{-1} dN/d \log \rho$ .

We have now all the ingredients necessary to compute the average magnification of sources located at a given redshift, for a generic detector network. Here we summarize the ingredients that enter the computation. We are focussing on (sufficiently)<sup>6</sup> low redshift sources for which the number density of sources per unit of signal to noise and as a function of redshift is given by

$$N(\rho, z_s) = \begin{cases} N_\rho(z_s)\rho^{-\gamma} & \text{for } \rho_1(z_s) < \rho < \rho_2(z_s), \\ 0 & \text{otherwise,} \end{cases} \quad (3.17)$$

where  $\gamma$  depends on the mass distribution for the two objects in the binary system as explained above and  $\rho_1 \equiv \rho_{\min}$ ,  $\rho_2 \equiv \rho_{\max}$  correspond to the minimum and maximum value of the SNR in a given redshift bin and are defined in eqs. (3.13) and (3.12). The number of sources which we see from redshift  $z_s$  with our limiting SNR  $\rho_{\text{lim}}$  when magnified by  $\mu$  is

$$\begin{aligned} N(\rho_{\text{lim}}, z_s, \mu) &= N_\rho(z_s) \int_{\alpha_{\text{lim}}}^{\rho_2(z_s)} d\rho \rho^{-\gamma} \\ &= \frac{N_\rho(z_s)}{\gamma - 1} \left[ \left( \frac{1}{\alpha_{\text{lim}}} \right)^{\gamma-1} - \left( \frac{1}{\rho_2(z_s)} \right)^{\gamma-1} \right], \end{aligned} \quad (3.18)$$

where  $\alpha_{\text{lim}} = \max(\rho_{\text{lim}}/\sqrt{\mu}, \rho_1(z_s))$ . We assume  $\rho_{\text{lim}}/\sqrt{\mu} < \rho_2(z_s)$ . If this is not the case,  $N(\rho_{\text{lim}}, z_s, \mu) = 0$ . We assume here that  $\gamma \neq 1$  but the case  $\gamma = 1$  can be easily worked out following steps similar to the ones performed below. The result without magnification is simply  $N(\rho_{\text{lim}}, z_s, 1)$ . The total number of sources which we see is therefore

$$N(\rho_{\text{lim}}, z_s) = \int_1^\infty d\mu p(\mu, z_s) N(\rho_{\text{lim}}, z_s, \mu). \quad (3.19)$$

With a bit of algebra this can be rewritten as

$$\begin{aligned} N(\rho_{\text{lim}}, z_s) &= \frac{N_\rho}{\gamma - 1} (\rho_1^{-\gamma+1} - \rho_2^{-\gamma+1}) + \frac{N_\rho}{\gamma - 1} \left[ \rho_2^{-\gamma+1} \int_1^{(\rho_{\text{lim}}/\rho_2)^2} d\mu p(\mu, z_s) \right. \\ &\quad \left. - \rho_1^{-\gamma+1} \int_1^{(\rho_{\text{lim}}/\rho_1)^2} d\mu p(\mu, z_s) + \int_{(\rho_{\text{lim}}/\rho_2)^2}^{(\rho_{\text{lim}}/\rho_1)^2} d\mu p(\mu, z_s) \left( \frac{\sqrt{\mu}}{\rho_{\text{lim}}} \right)^{\gamma-1} \right], \end{aligned} \quad (3.20)$$

where the redshift dependence in  $\rho_{1,2}$  and  $N_\rho$  is understood. We eventually want to compute the average magnification. For this we need to compute

$$M(\rho_{\text{lim}}, z_s) \equiv \int_1^\infty d\mu \mu p(\mu, z_s) N(\rho_{\text{lim}}, z_s, \mu), \quad (3.21)$$

which can be done with similar steps as above yielding

$$\begin{aligned} M(\rho_{\text{lim}}, z_s) &= \frac{N_\rho}{\gamma - 1} (\rho_1^{-\gamma+1} - \rho_2^{-\gamma+1}) \bar{\mu} + \frac{N_\rho}{\gamma - 1} \left[ \rho_2^{-\gamma+1} \int_1^{(\rho_{\text{lim}}/\rho_2)^2} d\mu \mu p(\mu, z_s) \right. \\ &\quad \left. - \rho_1^{-\gamma+1} \int_1^{(\rho_{\text{lim}}/\rho_1)^2} d\mu \mu p(\mu, z_s) + \int_{(\rho_{\text{lim}}/\rho_2)^2}^{(\rho_{\text{lim}}/\rho_1)^2} d\mu \mu p(\mu, z_s) \left( \frac{\sqrt{\mu}}{\rho_{\text{lim}}} \right)^{\gamma-1} \right], \end{aligned} \quad (3.22)$$

---

<sup>6</sup>We will come back to this point at the end of the next section. In particular, we will explain that this is a detector dependent condition. For LIGO-Virgo like sensitivity curve, this assumption holds for sources up to redshift of about 1.5, while for the Einstein Telescope (ET) it is valid up to much higher redshifts.

where  $\bar{\mu}$  depends on the source redshift and is defined as

$$\bar{\mu}(z_s) = \int_1^\infty d\mu \mu p(\mu, z_s). \quad (3.23)$$

The average magnification is now given by the ratio of (3.22) over (3.18)

$$\langle \mu \rangle(z_s) = M(\rho_{\text{lim}}, z_s) / N(\rho_{\text{lim}}, z_s). \quad (3.24)$$

Completely analogous steps can be performed working with the number density as a function of intrinsic luminosity (3.16), see the appendix for the explicit computation of magnification in this context.

Our analytic model for the distribution of sources has four free parameters:  $(\gamma, \mathcal{M}_{\text{min}}, \mathcal{M}_{\text{max}})$  defining the distribution of chirp masses and  $\rho_{\text{lim}}$  (or equivalently  $S_n$ ) which gives the minimum signal to noise for detection, and depends on the detector network chosen. The computation of the average magnification presented in this section relies on the assumption that we can replace the mass dependence of the ISCO frequency appearing in the expression of the SNR (3.10) by an average. From a comparison with numerical models of section 4, it turns out that this approximation is well justified from low redshift sources ( $z_s < 2$  when considering the sensitivity curve of the LIGO-Virgo detectors). The comparison is shown in Fig. 4. As already explained, the average magnification does not depend on the scaling of the number of events with redshift, i.e. on  $N_\rho(z_s)$  in eq. 3.17. To compare with a realistic population model, in Fig. 4 we have reconstructed this dependence fitting the numerical model, i.e.  $N_\rho(z_s) \propto \rho^{-3}$ . For high redshift sources a simple analytic derivation of the average magnification is not possible, but the relation (3.10) can be inverted numerically to find the chirp mass and the integrals (3.22) and (3.18) can be performed numerically to find the average magnification as a function of redshift.

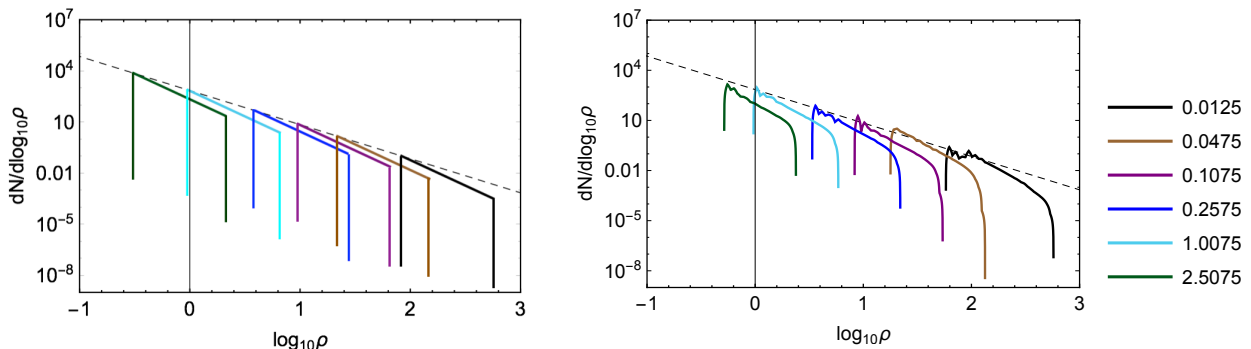


**Figure 4.** Comparison between the analytic model for source distribution presented in section 3.2 and the numerical simulations of section 4.3, for  $z < 2.5$ .

### 3.3 Analytical results for the LIGO detector(s)

In this section we focus on the case of the LIGO detectors and we compute the average magnification for different astrophysical models for the distribution of sources, corresponding to different choices



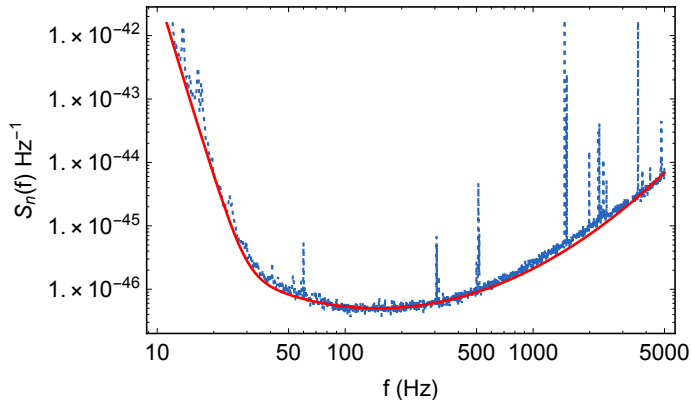


**Figure 5.** Spectral noise curve for the LIGO-Livingstone detector [17]. The red curve is the fit in eq. (3.25).

of the parameters  $(\gamma, \mathcal{M}_{\min}, \mathcal{M}_{\max})$ . For definiteness we consider the noise curve of the LIGO-Livingstone detector. In Fig. 5 we plot the spectral noise of the LIGO-Livingstone detector that we find to be well described by the fitting function  $S_{\text{fit}}(f)$  given by

$$S_{\text{fit}}(f) = \mathcal{A}_s \left[ \left( \frac{f}{30\text{Hz}} \right)^{\alpha_s} + 1 \right] \exp \left[ \beta_s \left( \log \left( \frac{f}{150\text{Hz}} \right) \right)^2 \right], \quad (3.25)$$

with  $\mathcal{A}_s = 10^{-46.3}$ ,  $\alpha_s = -7.8$  and  $\beta_s = 0.4$ .

We analyze the dependence of the average amplification on the details of the simple astrophysical model presented in last section. In particular, we want to explore the dependence on the distribution of the component masses and on the upper cut-off in the distribution. We assume the mass of the primary BH mass is distributed as  $p(m_1) \propto m_1^{-\alpha}$  in the range  $[5, X]M_\odot$  where both  $\alpha$  and  $X$  are two parameters that we vary. We consider two cases:  $\alpha = 2.35$  and  $\alpha = 1.5$ . The corresponding normalized distribution of chirp masses is shown in Fig. 6: the scaling is polynomial in the chirp mass, i.e.  $p(\mathcal{M}_c) \propto \mathcal{M}_c^{-\beta_M}$  with  $\beta_M = 3.2$  and  $\beta_M = 2.1$  respectively. As explained in the previous section, for sufficiently small redshift, the scaling of the number density of sources per unit of signal to noise is then given by (3.15) with  $\gamma = -1/5(1 - 6\beta_M)$ , hence  $\gamma = 3.6$  and  $2.3$  for the two values of  $\alpha$ , respectively.

In Fig. 6 we plot the normalized distribution of chirp masses while in Fig. 7 we show results for the average magnification as a function of redshift for the two models considered and for two different values of cut-off in the mass distribution. From a comparison with the numerical model of section 4, it turns out that this approximation is well justified for low redshift sources ( $z_s < 2$  when considering the sensitivity curve of the LIGO-Virgo detectors). As we will see in section 4.4, the result for the average amplification in Fig. 7 is in very good agreement with the one we find using a realistic model for source formation and evolution, for low redshift sources (see Fig. 20).

We have considered here the case of the LIGO-Livingston detector, but analogous results can be easily obtained for any other ground based detector (or detector network), just using the noise curve of that detector. For example, when using the Einstein Telescope (ET) where significantly lower frequencies and lower mass objects can be detected (see Fig. 15 for the noise curve), we expect that our analytical model can be extrapolated up to higher redshift. Comparing our analytical model with the numerical one, we find (see Section 4) that it is a reasonably good fit as long as

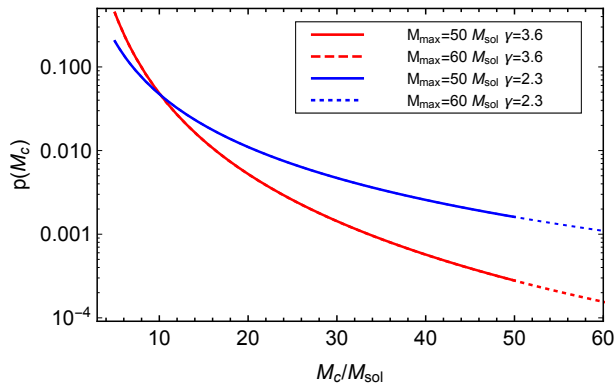


**Figure 6.** Probability distribution of chirp mass for both models with  $\alpha = 2.35$  and  $\alpha = 1.5$  (and correspondingly  $\gamma = 3.6$  and  $\gamma = 2.3$ ) and for the two cut-off in the primary mass distribution  $50M_\odot$  and  $60M_\odot$ .

high mass binaries have a higher SNR than low mass ones. For the ET which has much better sensitivity at 1-10Hz this remains true up to higher redshifts than for LIGO-Virgo.

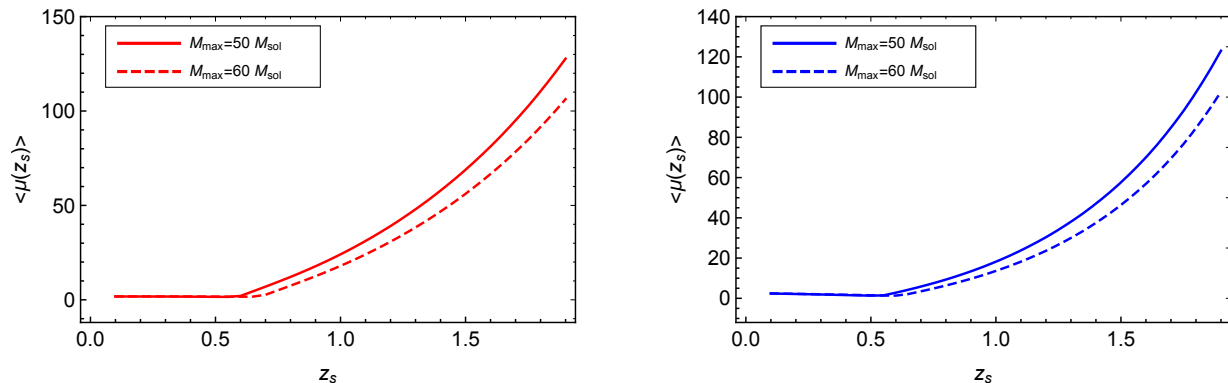


**Figure 7.** Left: Average magnification for  $\alpha = 2.35$  ( $\gamma = 3.6$ ) for two different upper cut-off in the distribution of the primary mass. Right: Average magnification for  $\alpha = 1.5$  ( $\gamma = 2.3$ ) for two different upper cut-off in the distribution of the primary mass.

## 4 Numerical results

In this section we model the distribution and redshift evolution of lenses (galaxies) using fits to hydrodynamical simulations, which we compare to fits to observations for  $z = 0$ . We also model the distribution of GW sources using a phenomenological model of the binary BH population.

### 4.1 The lens distribution

We model the number density of galaxies (lenses) as a function of the velocity dispersion  $n(\sigma_v, z)$ , taking into account the evolution of galaxies with redshift. For this, we use the results of Torrey et al. [18] based on the Illustris hydrodynamical simulation.

We use the values in Table 6 in the ArXiv version of Ref. [18], but we do not use the fitting formula given there. The correct fit is [19]

$$\log N(> \sigma_v, z) = A(z) + \alpha(z) \log \sigma_v - \gamma(z) + \beta(z) (\log \sigma_v - \gamma(z))^2 - \sigma_v \times 10^{-\gamma(z)} \quad (4.1)$$

where all logarithms are in base 10 and the numerical value of  $\sigma_v$  is to be taken in units of km/sec. The functions  $A$ ,  $\alpha$ ,  $\beta$  and  $\gamma$  are modeled as

$$A = a_0 + a_1 z + a_2 z^2, \quad (4.2)$$

$$\alpha = \alpha_0 + \alpha_1 z + \alpha_2 z^2, \quad (4.3)$$

$$\beta = \beta_0 + \beta_1 z + \beta_2 z^2, \quad (4.4)$$

$$\gamma = \gamma_0 + \gamma_1 z + \gamma_2 z^2. \quad (4.5)$$

For completeness we give the parameters  $a_0$  to  $\gamma_2$  in the Appendix. The central stellar velocity dispersion,  $\sigma_v$  is defined as the three-dimensional standard deviation of the stellar velocity within the stellar half-mass radius. We define

$$n(\sigma_v, z) \equiv -\frac{dN}{d\sigma_v}(> \sigma_v, z), \quad (4.6)$$

The result for different redshifts is shown in Fig. 8.

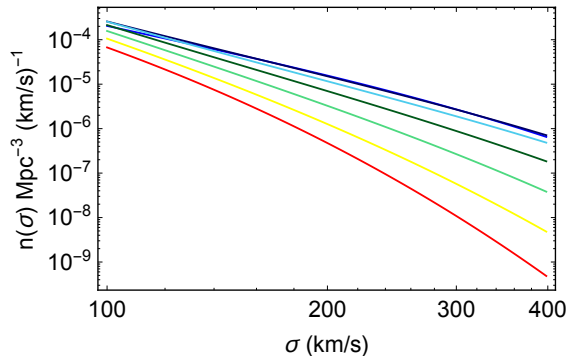


**Figure 8.** Number density of galaxies as a function of of velocity dispersion  $\sigma_v$  for different redshifts. The color code is:  $z = 0, 1, 2, 3, 4, 5, 6$  from black to red.

## 4.2 Results for optical depth and probability

To determine the optical depth given in (2.31), we need to compute the integral

$$\int d\sigma_v \sigma_v^4 n_{\text{phys}}(\sigma_v, z) = (1+z)^3 \int d\sigma_v \sigma_v^4 n(\sigma_v, z), \quad (4.7)$$

where we recall that  $\sigma_v^4$  is in units of  $(\text{km/s})^4 \sim 1.2 \cdot 10^{-22}$ . With this we can compute the cross-section, the optical depth and probability of lensing. In Fig. 9 we present the results for the cross-section given in eq. (2.27), as a function of the lens redshift and for different redshift of the GW source.

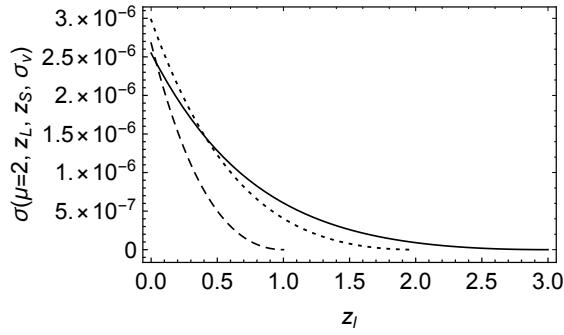


**Figure 9.** Cross section (in units of  $\text{Mpc}^2$ ) for  $\mu_1 = 2$  and  $\sigma_v = 63 \text{ km/s}$ , in a  $\Lambda\text{CDM}$  universe. Different curves are for different redshift of the source:  $z_s = 1, 2, 3$  (dashed, dotted and continuous respectively).

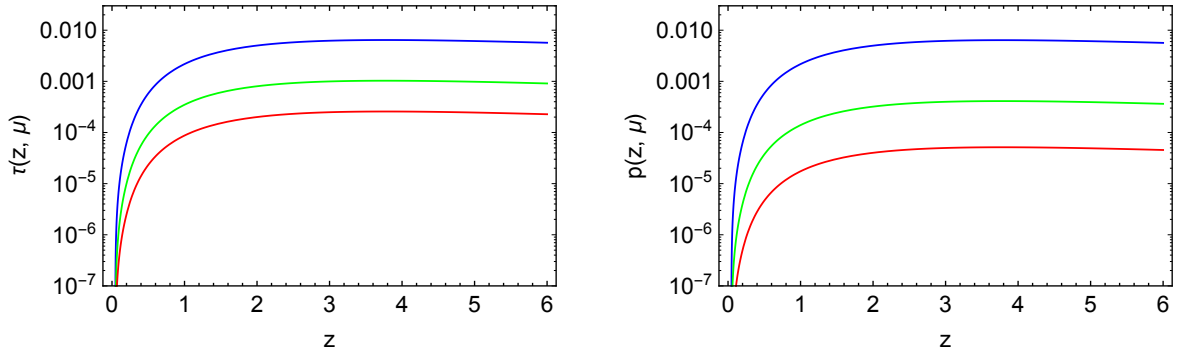


**Figure 10.** Left: Optical depth for  $\mu = 2, 5, 10$  (from top to bottom) using the lens distribution from (4.1). Right: Lensing probability density  $p(\mu, z)$  for  $\mu = 2, 5, 10$  (from top to bottom) using the lens distribution from (4.1).

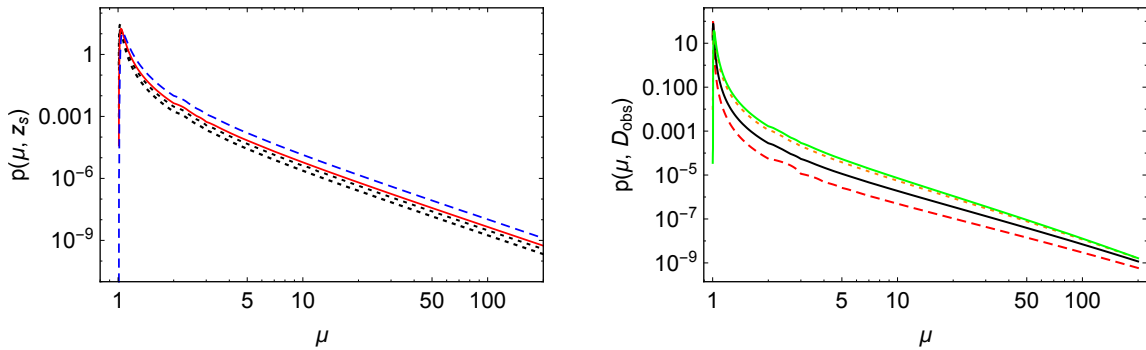


**Figure 11.** Left: Lensing probability density  $p(\mu, z_s)$  as a function of magnification for  $z = 0.6, 0.8, 1, 2$  (from bottom to top) using the Illustris result (4.1). Right: Lensing probability density  $p(\mu, D_{\text{obs}})$  as a function of magnification for  $D_{\text{obs}} = 500, 1000, 2000, 2300 \text{ Mpc}$  (from bottom to top) using the Illustris result (4.1).

In Fig. 10, we plot the optical depth for  $\mu = 2, 5, 10$  as a function of redshift on the left panel and the probability density on the right panel. The probability for lensing magnification even by just a factor of 2 always remains below 1%.

In Fig. 11 we plot the probability density as a function of the magnification for different redshifts. On the left hand panel we present curves for fixed source redshifts while in the right hand panel we fix the observer distance  $D_{\text{obs}} = \sqrt{\mu}D(z_s)$ . We have verified that the integral of each curve is one, hence the probability density is correctly normalized. We use fits to the Illustris simulation, eq. (4.1), to describe the redshift evolution of lenses. Note that the probability distribution is always strongly peaked at  $\mu \simeq 1$ . Only for  $D_{\text{obs}} = 2300$  does the probability for  $\mu = 2$  become close to 1%.

To have some intuition about the role of evolution we finally compare our result with a non-evolving lens distribution. For this we use the distribution function (4.1) for  $z = 0$  assuming no redshift evolution. We then have

$$n_{\text{phys}}(\sigma_v, z) = (1 + z)^3 n(\sigma_v, z = 0). \quad (4.8)$$

Then we compute the optical depth and probability of lensing for the case of no evolution of lenses with time. In figure 12 we plot the relative difference between the probability density with evolution as given in (4.1) and without redshift evolution. The result is valid for arbitrary magnification  $\mu$ .

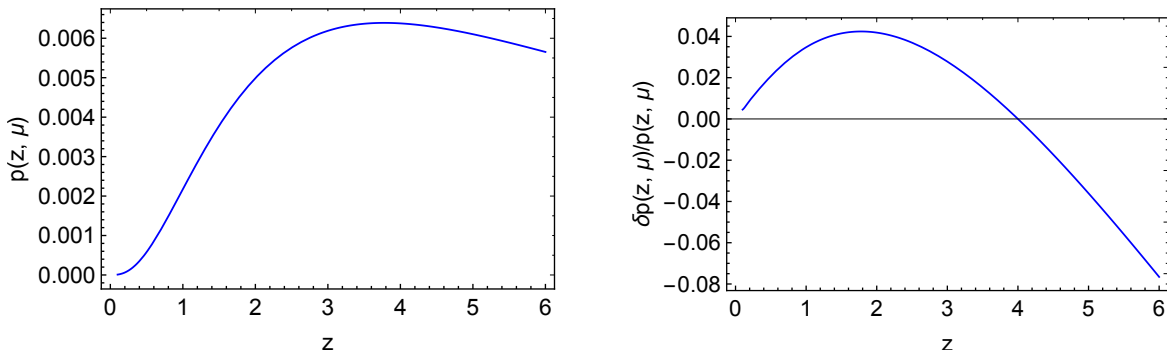


**Figure 12.** Left : The lensing probability density  $p(\mu, z)$  as a function of redshift for  $\mu = 2$  using the Illustris result (4.1). Right: The relative difference between the probability with and without redshift evolution. The result is valid for arbitrary magnification  $\mu$ .

At low redshift,  $0 < z < 2$ , the non evolving distribution actually has somewhat less galaxies with low velocity dispersion which are the most numerous ones and therefore the evolving distribution leads to a higher probability for magnification than the non-evolving one,  $\delta P > 0$ . At higher redshift,  $z > 4$  the loss of lenses in the evolving distribution becomes more relevant and  $\delta P$  changes sign. But the difference between the evolving and non-evolving distribution is never larger than 8% for redshift  $z \leq 6$ . This tells us that our results are quite insensitive to the redshift evolution of the lenses.

### 4.3 Modeling the distribution of GW sources

Let us now describe the modeling of the GW sources. As in Section 3.2 we will concentrate on short-lived sources, such as compact binary coalescences which can be observed with LIGO-Virgo

[1–6, 8]. Interestingly, the first detections of binary black holes (BBHs) revealed a population of sources more massive than those known from X-ray binaries, with masses of up to  $50M_\odot$  discovered during the second LIGO observation run [6, 8]. Such high masses are in fact predicted by various stellar evolution models [20–29, e.g.]. Nevertheless, these findings inspired the authors of Ref. [10] to suggest that the intrinsic masses of the observed BBHs were much lower, closer to the ones found in X-ray binaries, and the apparent high masses are the result of redshifting, implying that these are high-redshift sources that underwent gravitational lensing. The detailed analysis of the individual events in Ref. [11] found that the probability of lensing for the sources observed by LIGO-Virgo so far is vanishingly small, with the consequence that BH population models can be reasonably informed by GW observations to date, as summarized in the first GW source catalogue [8, 30]. In this work we shall confirm this finding with a statistical analysis.

We focus below on BBH events and assume that their masses are in the range  $[5, 50]M_\odot$  [8, 30]. We further assume that their formation rate is proportional to the cosmic star formation rate (SFR), for which we use the following parametric from [31]:

$$\Psi(t(z)) = A \frac{e^{b(z-z_m)}}{a - b + b \cdot e^{a(z-z_m)}}, \quad (4.9)$$

with  $A = 0.24M_\odot/\text{yr}/\text{Mpc}^3$ ,  $z_m = 2.3$ ,  $a = 2.2$  and  $b = 1.4$ . Note that we use this parametrization in the redshift range  $[0, 20]$  even though it was derived using observations up to  $z = 9$ . We define an efficiency parameter  $\epsilon$  to describe the fraction of mass in BBH that merge within the age of the Universe that form out of a given stellar population. Moreover, we assume a delay time  $t_{\text{delay}}$  between the formation of the progenitor star and the coalescence of the BBH, where the latter is distributed as

$$P_d(t_{\text{delay}}) \propto t_{\text{delay}}^{-1}, \quad (4.10)$$

in the range  $[t_{\text{min}}, t_{\text{max}}]$  with  $t_{\text{min}} = 50$  Myr and  $t_{\text{max}}$  equal to the age of the Universe. We also assume that the mass of the primary BH is distributed as:

$$P(m_1) \propto m_1^{-\alpha}, \quad (4.11)$$

in the range  $[5, 50]M_\odot$  with  $\alpha = 2.35$ , while the mass of the secondary BH is uniformly distributed in the range  $[5, m_1]$  so that  $p(m_2) = \text{const.}$  in this range and  $p(m_1, m_2) = p(m_1)p(m_2)$  [30] (note that this mass distribution is independent of redshift). We assume zero spins for all the BHs. The merger rate is then given by the following integral over the delay time distribution:

$$\frac{dR}{dm_1 dm_2 dz} = \epsilon T_{\text{obs}} \int \Psi(t(z) - t_{\text{delay}}) p(m_1, m_2) P_d(t_{\text{delay}}) \frac{dV}{dz dt_{\text{delay}}}. \quad (4.12)$$

We then calculate the SNR of each merger by using eq. (2.37). We use the *PhenomB* inspiral-merger-ringdown waveforms to calculate the strain [32] and we use the noise power spectral density publicly available from [33, 34]. We consider the event observable if it has  $\rho \geq \rho_{\text{lim}} = 10$ . The normalization parameter  $\epsilon$  is obtained by comparing the number of observable events in our model to the number of events observed during the first two LIGO/Virgo observational campaigns O1+O2:

$$N_{\text{obs}} = \int_{\rho(m_1, m_2, z) \geq 10} \frac{dR}{dm_1 dm_2 dz} dm_1 dm_2 dz \quad (4.13)$$

where  $N_{\text{obs}} = 10$  and  $T_{\text{obs}} = 170$  days. The merger rate per unit redshift and SNR is then calculated from eq. (4.12).

In Fig. 13 we show the number of GW events per unit of SNR in different redshift bins. We observe that at low redshift the slope and the width of the curves is constant, as expected from the analytic analysis of Section 3. At high redshift curves develop a low-SNR tail. The reason for this can be understood from Fig. 15 where we plot the characteristic strain of BBH mergers with two different values of the chirp mass (left and right panel) and for different redshifts, together with the LIGO detector noise (black solid) and the ET detector noise (black dashed). At low redshift, the SNR of high-mass events is always bigger than the one of low-mass events due to their higher amplitude. At high redshift, however, the sharp increase of the noise curve at low frequencies reduces the SNR of high masses more than the one of low masses which have higher frequencies so that the situation becomes actually reversed and low masses have a higher SNR. This leads to a spread of the SNR for different events over a large range. Of course for all masses at high redshift the SNR is very small and they can only be observed if they are highly magnified.

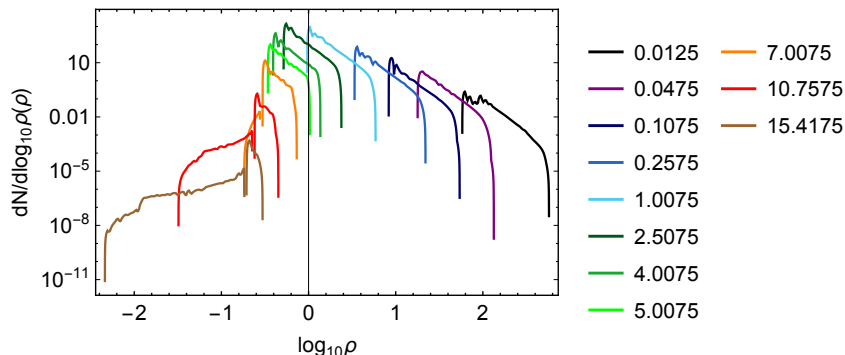


**Figure 13.** Number of events per unit of  $\log_{10}\text{SNR}$ . Each line corresponds to the number of events in a redshift bin  $z \pm 0.025$  and the values of redshift are listed in the legend on the right.

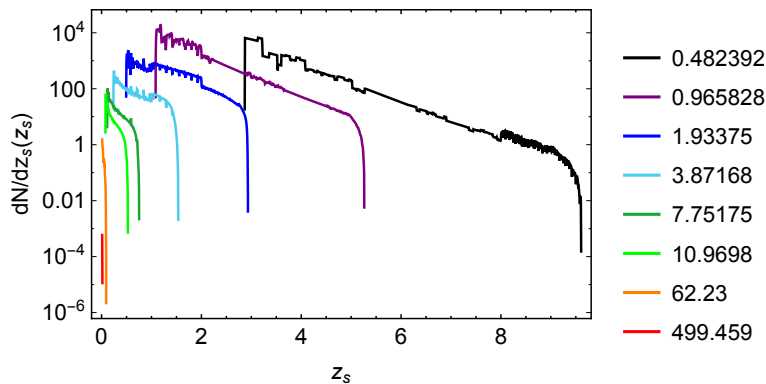


**Figure 14.** Number of events per unit of redshift. Each line corresponds to the number of events in a bin of signal-to-noise  $\log_{10}\text{SNR} \pm 0.015$  and the values of  $\rho$  are listed in the legend on the right of the figure.

#### 4.4 The average amplification

In Fig. 16 we present the number density of magnified objects per unit of observed luminosity distance, as a function of the magnification, for different  $D_{\text{obs}}$ . In the right panel of the figure we

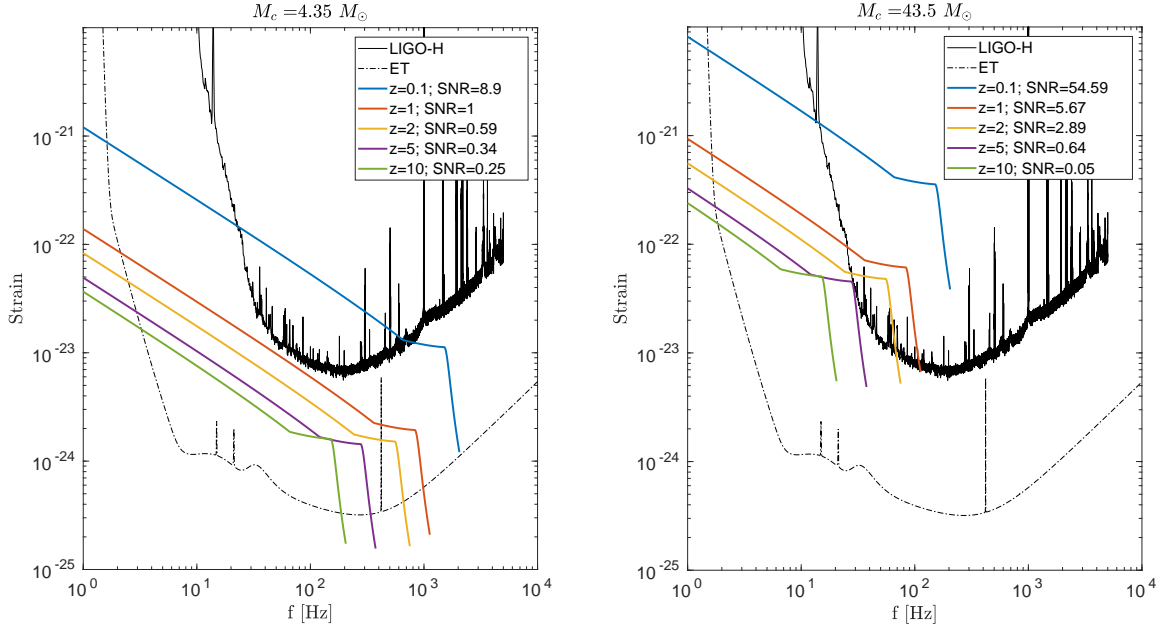


**Figure 15.** We fix in each panel a value of the chirp mass and we plot the strain for sources with that mass and in different redshift bins. The solid black curve is the strain sensitivity of the LIGO-Hanford detector [34], the dashed-dotted curve is the strain sensitivity of the Einstein Telescope [35].

multiply the result by the probability density of lensing as a function of luminosity distance and magnification. In Fig. 17 we plot the same quantities for different values of the intrinsic redshift of the source. In Fig. 18 we show the probability distribution (2.44) as a function of amplification, for two different values of redshift. We see that the peak of the distribution moves towards high values of the magnification as we increase the intrinsic redshift. In Fig. 19 we plot the the probability distribution (2.50) as a function of amplification, for two different values of the observed luminosity distance. In Fig. 20 we present the results for the amplification factor as a function of real redshift and luminosity distance of the sources (left and right panels respectively), while in Fig. 21 we present the results for the amplification factor as a function of observed redshift and luminosity distance of the sources (left and right panels respectively). No sources are observable beyond 5500 Mpc.<sup>7</sup>

The minimum amplification needed to detect sources from a redshift  $z_s$  and with a given  $\rho_{\max}(z_s) < \rho_{\lim}$  is given by

$$\mu_{\min}(z_s) = \left( \frac{\rho_{\lim}}{\rho_{\max}} \right)^2, \quad (4.14)$$

<sup>7</sup>This can be understood computing the probability of seeing a source from a given observed distance, i.e. integrating  $p(\mu, D_{\text{obs}})$  over  $\mu$ . The probability of seen an object from distance bigger than 5000 Mpc is smaller than  $10^{-7}$ .



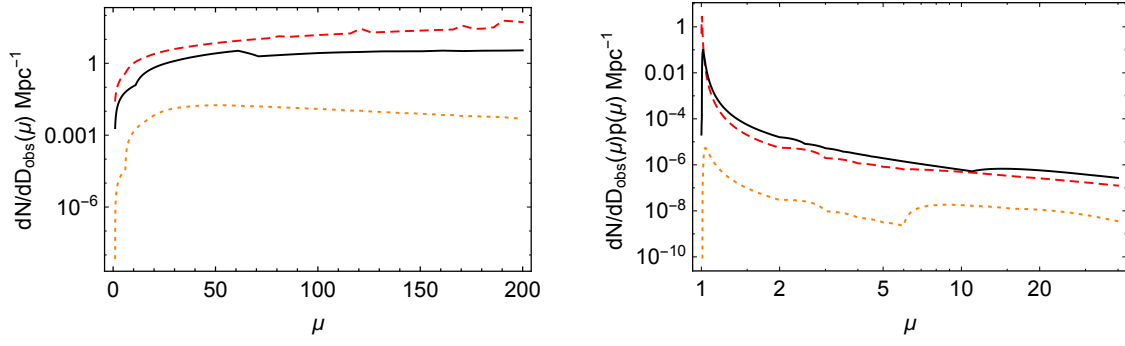


**Figure 16.** Left: Number of events per unit of  $\text{Mpc}^{-1}$  with magnification  $\mu$  as a function of  $\mu$ , for different observed luminosity distance:  $D_{\text{obs}} = (500, 2000, 4500)$  Mpc, black, red and orange curve, respectively. This quantity is given by  $dN/dD_{\text{obs}}$  in eq. (2.48). Right: The same quantity multiplied by  $p(\mu, D_{\text{obs}})$  to obtain the probability distribution in eq. (2.50) per unit of observed distance.

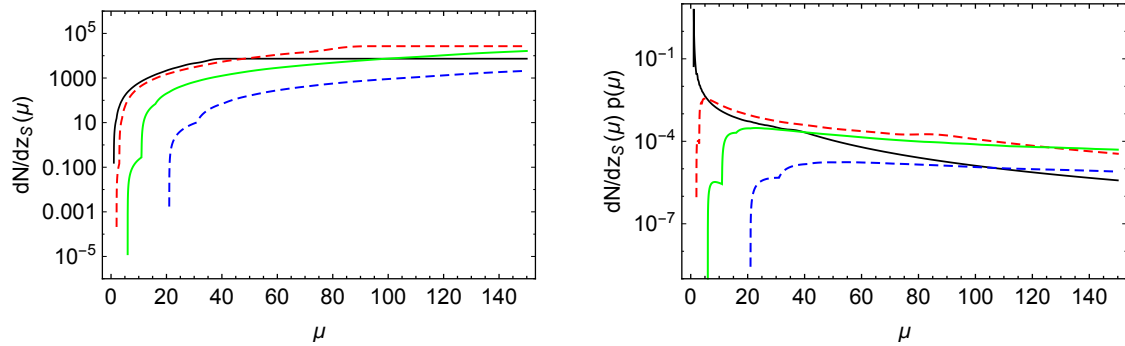


**Figure 17.** Left: Number of events per unit of redshift with magnification  $\mu$  as a function of  $\mu$ , for different *true* redshift:  $z = (0.6, 1, 2, 3)$  black, red, green, blue line respectively. This quantity is given by  $dN/dz_s$  in eq. (2.42). Right: Same quantity multiplied by  $p(\mu, z_s)$  to obtain the probability distribution (per unit of redshift) in eq. (2.44).

hence we can see sources from a maximum observed distance given by

$$D_{\text{obs}}^{\text{max}}(z_s) = \frac{D(z_s)}{\sqrt{\mu_{\text{min}}}} = \frac{D(z_s)\rho_{\text{max}}(z_s)}{\rho_{\text{lim}}}. \quad (4.15)$$

For low redshifts,  $z \lesssim 2$  we can work out the scaling of this quantity with redshift from our simple model just using eq. (3.12). We find

$$D_{\text{obs}}^{\text{max}}(z_s) = \frac{\mathcal{A}}{\rho_{\text{lim}}} \left( \frac{\mathcal{M}_{\text{max}}}{M_{\odot}} \right)^{5/6} (1+z_s)^{5/6} f_{7/3}(z_s)^{1/2} \text{Mpc}. \quad (4.16)$$

For higher redshift our model becomes too inaccurate and this scaling is no longer valid.

## 5 Discussion and conclusion

Due to the cosmological expansion, the frequencies of gravitational waves are redshifted. Since the frequencies from BBH collisions are degenerate with the masses, the quantity that we measure

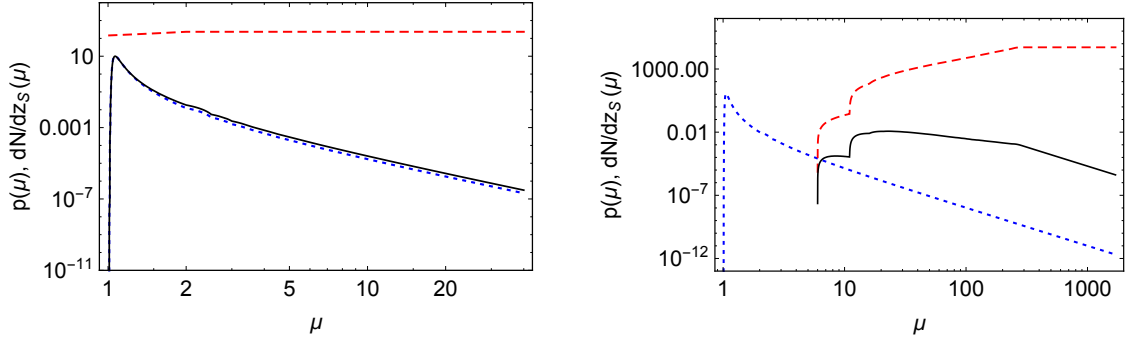


**Figure 18.** Number of events per unit of redshift with magnification  $\mu$  as a function of  $\mu$  (red dashed line), together with  $p(\mu, z_s)$  (blue dotted line) and the normalized probability distribution of  $\mu$   $\mathcal{P}_s(\mu)$  see eq. (2.44), proportional to their product (black line). In the left panel we chose  $z_s = 0.1$  in the right  $z_s = 2$ .

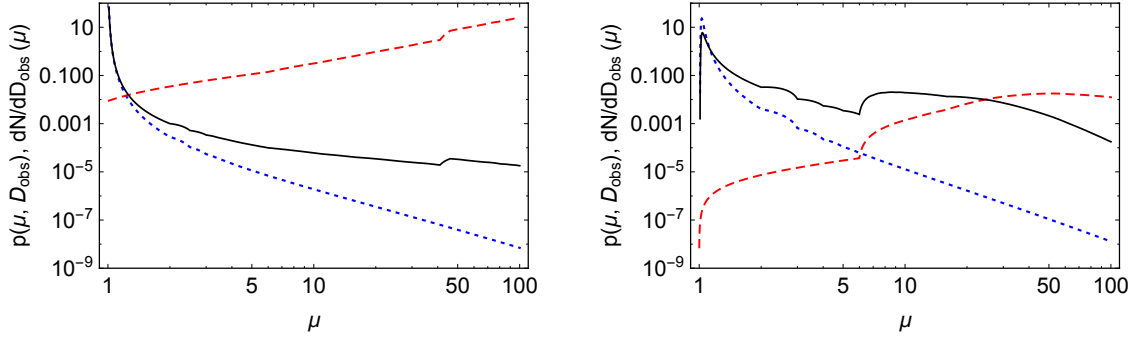


**Figure 19.** Number of events per unit of observed distance with magnification  $\mu$  as a function of  $\mu$  (red dashed line), together with  $p(\mu, D_{\text{obs}})$  (blue dotted line) and the normalized probability distribution of  $\mu$ ,  $\mathcal{P}_{\text{obs}}(\mu)$  see eq. (2.50), proportional to their product (black line). In the left panel we chose  $D_{\text{obs}} = 1000$  Mpc in the right  $D_{\text{obs}} = 4500$  Mpc.

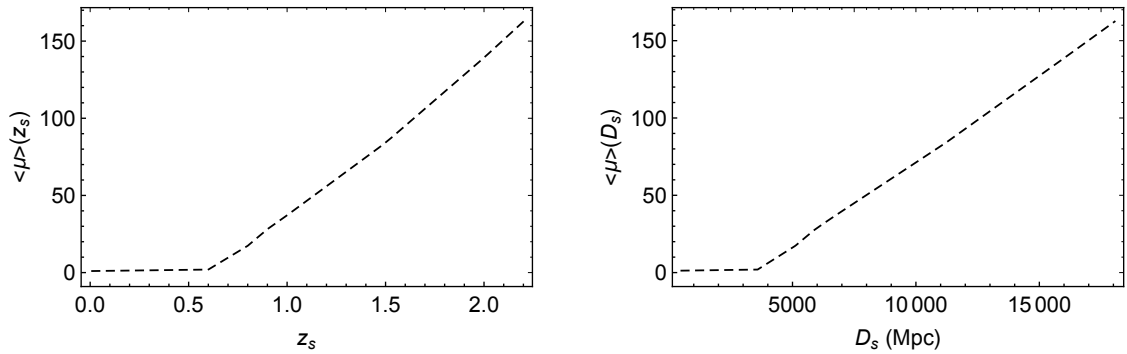


**Figure 20.** Amplification factor for events observable by LIGO-Virgo as a function of *true redshift* of a source (left) and as a function of the true luminosity distance (right).

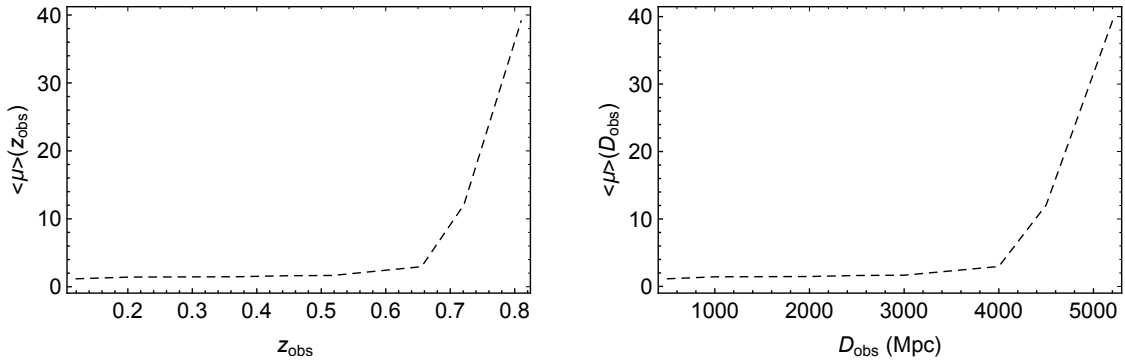


**Figure 21.** Amplification factor for events observable by LIGO-Virgo, as a function of *observed redshift* of a source (left) and as a function of the observed luminosity distance (right).

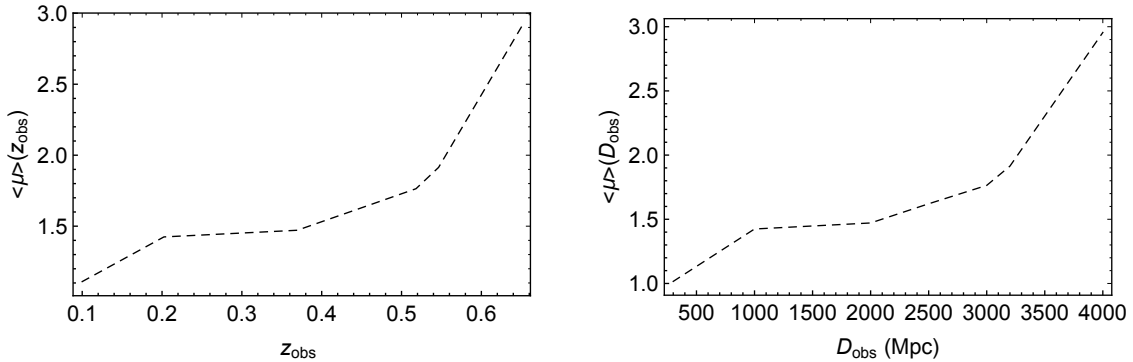


**Figure 22.** Amplification factor for events observable by LIGO-Virgo, as a function of *observed redshift* of a source (left) and as a function of the observed luminosity distance (right). This is a zoom on the low redshift part of [21](#).

directly from the signal is the redshifted chirp mass  $\mathcal{M}_z = (1 + z)\mathcal{M}$ , where  $\mathcal{M}$  is the intrinsic (true) chirp mass of the binary at a redshift  $z$ . The estimated luminosity distance can be converted into a redshift estimate (choosing a cosmological model), which can, in turn be used to estimate the intrinsic chirp mass  $\mathcal{M}$  of the binary. The unknown lensing magnification will bias our estimation of the intrinsic mass and the distance (or equivalently, the redshift) of the binary. Therefore, lensed binaries will appear as a population of lower redshift and higher mass sources.

In this article we have proposed a semi-analytical approach to study weak and strong lensing of gravitational waves by galaxies. We presented a fully analytical model to study the dependence of the result on the choice of the distribution of lenses and of the distribution and luminosity of sources. The framework we proposed can be applied to any detector or detector network once the strain noise of the observatory is known. We also developed a more complete numerical study to include a realistic evolution of the lenses with time. We presented results for the probability of strong lensing as a function of redshift and magnification and for the average amplification as a function of real and observed distance.

Results for the probability of a magnification  $\mu$  as a function of both intrinsic and observed

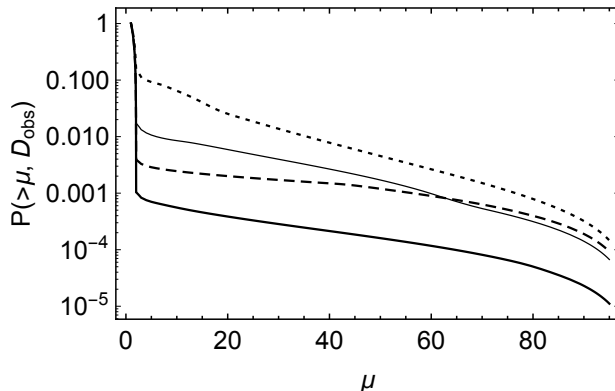


**Figure 23.** Probability that a given GW event observed by LIGO-Virgo has magnification bigger than a given value  $\mu$ , as a function of  $\mu$ , for different observed distances  $D_{\text{obs}} = 500, 1000, 2000, 4000$ , from bottom to top respectively.

redshift (or rather distance) of a source, are presented in Fig. 11. We stress that this result does not depend on the properties of the distribution of sources, nor on the specifics of a given observatory. The probability is small, but it decays slowly as a function of magnification. More specifically, for large values of the magnification, the probability as a function of intrinsic redshift scales as  $p(\mu, z_s) \propto \mu^{-3}$ . This scaling is independent of the lens distribution model. The probability density as a function of the observed distance,  $p(\mu, D_{\text{obs}}) \equiv p(\mu, z_s(\sqrt{\mu}D_{\text{obs}}))$  has an even slower decay with magnification, see right panel of Fig. 11. Indeed, for a fixed  $D_{\text{obs}}$  and  $\mu > 1$ ,  $p(\mu, D_{\text{obs}}) \equiv p(\mu, z_s(\sqrt{\mu}D_{\text{obs}}))$  comes from a higher redshift than  $z_s(D_{\text{obs}})$  and is therefore larger. The exact scaling of  $p(\mu, D_{\text{obs}})$  with  $\mu$  depends on the details of the lens distribution. For a realistic distribution with a comoving number density of lenses which fits numerical simulations (Illustris), we find that  $p(\mu, D_{\text{obs}}) \propto \mu^{-\alpha}$ . The value of  $\alpha$  increases from 2.2 to 3 as the observed luminosity distance varies from  $\sim 300\text{Mpc}$  to  $1500\text{Mpc}$  where it saturates to the asymptotic value  $\alpha = 3$ . From Fig. 11 we read the probability that a source with observed luminosity distance of  $D_{\text{obs}} = 2000$  Mpc is magnified of  $\mu = 2$ ,  $p(2, 2000\text{Mpc}) \simeq 0.01$ . The probability that a source observed from this same distance is magnified of  $\mu = 10$  is  $10^{-4}$ . Notice that this result is detector-independent.

Selection effects related to the sensitivity curve (hence to the horizon) of a given detector network enter into the game when computing the probability that a source *that we can observe* with a given observatory has a given magnification. This probability distribution  $\mathcal{P}_{\text{obs}}(\mu)$ , is defined in eqs. (2.44) and (2.50) as function of the intrinsic redshift of a source and as function of the observed luminosity distance respectively. We focussed on the LIGO-Virgo network in our analysis. Plots of the distribution of magnification for different intrinsic redshifts and observed luminosity distance are presented in Figs. 18 and 19. The distribution is highly peaked at  $\mu = 1$  for low observed distances and the peak starts to spread out as we move towards higher redshift. The integral of this distribution multiplied by  $\mu$  gives the average magnification expected for a given observed distance and the given observatory.

The probability distribution of magnification  $\mathcal{P}_{\text{obs}}(\mu)$  for a given observed distance, scales as  $\mathcal{P}_{\text{obs}}(\mu) \propto \mu^{-\alpha+1/2}$  and its integral from  $\mu$  to infinity behaves as  $\mathcal{P}_{\text{obs}}(> \mu) \propto \mu^{-\alpha+3/2}$  for large values of  $\mu$ , with  $\alpha \in [2.3, 3]$ . The probability,  $\mathcal{P}_{\text{obs}}(> \mu)$  is presented in Fig. 23 for different values of  $D_{\text{obs}}$ . From this scaling, it follows that the mean of the magnification at small observed distances

diverges at large  $\mu$ . This is due to the presence of rare but extremely highly magnified sources, i.e. sources aligned along the lens-observer direction for which the magnification  $\mu \rightarrow \infty$ , see eq. (2.24). Physically, the magnification tends to a finite value and, as mentioned above, the presence of the divergence is due to the geometric optics approximation, which breaks down in the vicinity of caustics, where wave effects need to be taken into account. Nevertheless, this indicates that the distribution has a significant tail with large magnification. That the mean of the magnification diverges only for small observed distances is due to the fact that highly magnified sources appear to have small distances<sup>8</sup>,  $D_{\text{obs}} = D_s/\sqrt{\mu}$ . In Figs. 20 to 22 we present the average amplification<sup>9</sup>. It is very close to 1 for low redshift and it starts growing from  $z_{\text{obs}} = 0.6$ , reaching the maximum value of 40 at a redshift 0.8 where we stop seeing sources, i.e. where the horizon of the observatory (computed allowing for the presence of magnification) lies.

In Section 3 we have analyzed the dependence of the magnification of detected sources on the details of the population of sources, i.e. on the distribution of masses of objects in binary systems, from a simple analytic model that captures the main dependences. This analysis, valid for low redshift sources, shows that the average magnification depends (mildly) on the details of the source population, but that the qualitatively picture of Fig. 21 is expected to be valid independently on the details of the astrophysical model chosen. The results for the average magnification as a function of intrinsic redshift that we find with the analytic model is in very good agreement with the result of the numerical analysis.

Let us finally derive some consequences for LIGO-Virgo O1 and O2 observations. The 10 observed BBH events have distances  $D_{\text{obs}} \in [320, 2750]\text{Mpc}$ . From Fig. 23 it follows that the probability that one of them has been magnified by magnification of 5 or bigger is  $\mathcal{P}_{\text{obs}}(> 5) \sim 0.01$ . However, the probability that magnification of one of them is bigger than 50 is not much smaller, namely  $\mathcal{P}_{\text{obs}}(> 50) \sim 0.005$ .

In this article we have presented a general framework to study lensing of GW by galaxies with a statistical approach. The framework is flexible and can be adapted to study strong and weak lensing of sources in any frequency band, and it can be applied to any detector network. We have presented quantities such as the probability of magnification as a function of intrinsic or observed redshift, which do not depend on instrumental details, but only on the lens model. We have then presented results for the probability that a given observed event has been magnified by a given amount. This quantity depends on the details of the observatory considered (on its sensitivity curve). In this work we have applied our formalism to the case of the LIGO-Virgo detectors. A future work will be dedicated to a detailed study of the ET and LISA cases, using the framework presented here.

## Acknowledgements

It is a pleasure to thank Michele Maggiore for helpful discussions. We also thank Paul Torrey for providing us with the analytic fitting formula of [18]. This project has received funding from

---

<sup>8</sup>It also follows that, for any fixed value of  $D_{\text{obs}}$  the variance of the distribution diverges as  $\mu^{-\alpha+7/2}$ . We stress that this is a general property of the probability distribution of magnification (for different observed redshift), independent on the details of the distribution of sources. Moreover, it applies also to the case of strongly lensed sources of electromagnetic radiation. Also in that case, the variance of the distribution of magnification (for different observed redshift) is divergent.

<sup>9</sup>A cut-off has been introduced to compute the mean for sources at low distances  $D_{\text{obs}} < 1000 \text{ Mpc}$ .

the European Research Council (ERC) under the European Union's Horizon 2020 research and innovation program (grant agreement No 693024) and from the Swiss National Science Foundation.

## A Fit to the Illustris simulation

In the following table we list the coefficients of the fitting formula used in Sec. 4.1 to describe the evolution of galaxy as a function of redshift and velocity dispersion [19].

$i$	$i = 0$	$i = 1$	$i = 2$
$A_i$	7.391498	5.729400	-1.120552
$\alpha_i$	-6.863393	-5.273271	1.104114
$\beta_i$	2.852083	1.255696	-0.286638
$\gamma_i$	0.067032	-0.048683	0.007648

## B Analytic model: Amplification as function of the luminosity

We derive here the analytic expression of the amplification as a function of redshift assuming that what it is known is the distribution of sources per unit of intrinsic luminosity and redshift. Our starting point is Summarizing, we consider the following expression for the number density of sources as a function of luminosity and redshift

$$N(L, z_s) = \begin{cases} N_L(z_s)L^{-\beta} & \text{for } L_1(z_s) < L < L_2(z_s), \\ 0 & \text{otherwise,} \end{cases} \quad (\text{B.1})$$

where  $\beta$  depends on the mass distribution for the two objects in the binary system as explained above. In eq. B.1,  $L_1$  and  $L_2$  correspond to the minimum and maximum value of the luminosity in a given bin, and can be easily related to the minimum and maximum signal to noise (considering a given detector) making use of eqs. 3.6 and 3.7. The number of sources which we see from redshift  $z_s$  with our limiting flux  $F_{\text{lim}} \propto \rho_{\text{lim}}^2$  when magnified by  $\mu$  is

$$\begin{aligned} N(F_{\text{lim}}, z_s, \mu) &= \int_{\alpha_{\text{lim}}}^{\infty} dL N_L(z_s)L^{-\beta} \\ &= \frac{1}{\beta - 1} N_L(z_s) \left[ \left( \frac{1}{\alpha_{\text{lim}}} \right)^{\beta-1} - \left( \frac{1}{L_2(z_s)} \right)^{\beta-1} \right], \end{aligned} \quad (\text{B.2})$$

where  $\alpha_{\text{lim}} = \max(L_{\text{lim}}/\mu, L_1(z_s))$ . We are here assuming that  $\beta \neq 1$  but the case  $\beta = 1$  can be easily worked out following steps similar to the ones proposed below. Without magnification this is simply  $N(F_{\text{lim}}, z_s, 1)$ . The total number of sources which we see is therefore

$$N(F_{\text{lim}}, z_s) = \int_1^{\infty} d\mu p(\mu, z_s) N(F_{\text{lim}}, z_s, \mu). \quad (\text{B.3})$$

With a bit of algebra this can be rewritten as

$$\begin{aligned} N(F_{\text{lim}}, z_s) &= \frac{N_L}{\beta - 1} (L_1^{-\beta+1} - L_2^{-\beta+1}) \\ &+ \frac{N_L}{\beta - 1} \left[ L_2^{-\beta+1} \int_1^{L_{\text{lim}}/L_2} d\mu p(\mu, z_s) - L_1^{-\beta+1} \int_1^{L_{\text{lim}}/L_1} d\mu p(\mu, z_s) + \int_{L_{\text{lim}}/L_2}^{L_{\text{lim}}/L_1} d\mu p(\mu, z_s) \left( \frac{\mu}{L_{\text{lim}}} \right)^{\beta-1} \right], \end{aligned} \quad (\text{B.4})$$

where to make the notation compact the redshift dependence in  $L_{1,2}$  and  $N_L$  is understood. We eventually want to compute the average magnification. For this we need to compute

$$M(F_{\text{lim}}, z_s) \equiv \int_1^\infty d\mu \mu p(\mu, z_s) N(F_{\text{lim}}, z_s, \mu), \quad (\text{B.5})$$

which can be done with similar steps and gives

$$M(F_{\text{lim}}, z_s) = \frac{N_L}{\beta - 1} (L_1^{-\beta+1} - L_2^{-\beta+1}) \bar{\mu} + \frac{N_L}{\beta - 1} \left[ L_2^{-\beta+1} \int_1^{L_{\text{lim}}/L_2} d\mu \mu p(\mu, z_s) - L_1^{-\beta+1} \int_1^{L_{\text{lim}}/L_1} d\mu \mu p(\mu, z_s) + \int_{L_{\text{lim}}/L_2}^{L_{\text{lim}}/L_1} d\mu \mu p(\mu, z_s) \left( \frac{\mu}{L_{\text{lim}}} \right)^{\beta-1} \right], \quad (\text{B.6})$$

where

$$\bar{\mu} = 2p_1 \int_1^\infty \frac{d\mu \mu}{(\mu - 1)^3} e^{-\frac{p_1}{(\mu-1)^2}}, \quad (\text{B.7})$$

and the average magnification is just given by (B.6) over (B.4)

$$\langle \mu \rangle(z_s) = M(F_{\text{lim}}, z_s) / N(F_{\text{lim}}, z_s). \quad (\text{B.8})$$

## References

- [1] **LIGO Scientific, Virgo** Collaboration, B. P. Abbott et al., *Observation of Gravitational Waves from a Binary Black Hole Merger*, *Phys. Rev. Lett.* **116** (2016), no. 6 061102, [[arXiv:1602.03837](#)].
- [2] **LIGO Scientific, Virgo** Collaboration, B. P. Abbott et al., *GW151226: Observation of Gravitational Waves from a 22-Solar-Mass Binary Black Hole Coalescence*, *Phys. Rev. Lett.* **116** (2016), no. 24 241103, [[arXiv:1606.04855](#)].
- [3] **LIGO Scientific, Virgo** Collaboration, B. P. Abbott et al., *Binary Black Hole Mergers in the first Advanced LIGO Observing Run*, *Phys. Rev.* **X6** (2016), no. 4 041015, [[arXiv:1606.04856](#)]. [erratum: *Phys. Rev.*X8,no.3,039903(2018)].
- [4] **LIGO Scientific, Virgo** Collaboration, B. P. Abbott et al., *GW170608: Observation of a 19-solar-mass Binary Black Hole Coalescence*, *Astrophys. J.* **851** (2017), no. 2 L35, [[arXiv:1711.05578](#)].
- [5] **LIGO Scientific, Virgo** Collaboration, B. P. Abbott et al., *GW170814: A Three-Detector Observation of Gravitational Waves from a Binary Black Hole Coalescence*, *Phys. Rev. Lett.* **119** (2017), no. 14 141101, [[arXiv:1709.09660](#)].
- [6] **LIGO Scientific, VIRGO** Collaboration, B. P. Abbott et al., *GW170104: Observation of a 50-Solar-Mass Binary Black Hole Coalescence at Redshift 0.2*, *Phys. Rev. Lett.* **118** (2017), no. 22 221101, [[arXiv:1706.01812](#)]. [Erratum: *Phys. Rev. Lett.*121,no.12,129901(2018)].
- [7] **Virgo, LIGO Scientific** Collaboration, B. Abbott et al., *GW170817: Observation of Gravitational Waves from a Binary Neutron Star Inspiral*, *Phys. Rev. Lett.* **119** (2017), no. 16 161101, [[arXiv:1710.05832](#)].
- [8] **LIGO Scientific, Virgo** Collaboration, B. P. Abbott et al., *GWTC-1: A Gravitational-Wave Transient Catalog of Compact Binary Mergers Observed by LIGO and Virgo during the First and Second Observing Runs*, *Phys. Rev.* **X9** (2019), no. 3 031040, [[arXiv:1811.12907](#)].
- [9] M. Oguri, *Effect of gravitational lensing on the distribution of gravitational waves from distant binary black hole mergers*, *Mon. Not. Roy. Astron. Soc.* **480** (2018), no. 3 3842–3855, [[arXiv:1807.02584](#)].



- [10] T. Broadhurst, J. M. Diego, and G. Smoot, *Reinterpreting Low Frequency LIGO/Virgo Events as Magnified Stellar-Mass Black Holes at Cosmological Distances*, [arXiv:1802.05273](#).
- [11] O. A. Hannuksela, K. Haris, K. K. Y. Ng, S. Kumar, A. K. Mehta, D. Keitel, T. G. F. Li, and P. Ajith, *Search for gravitational lensing signatures in LIGO-Virgo binary black hole events*, *Astrophys. J.* **874** (2019), no. 1 L2, [[arXiv:1901.02674](#)]. [*Astrophys. J. Lett.*874,L2(2019)].
- [12] M. Oguri, *Strong gravitational lensing of explosive transients*, [arXiv:1907.06830](#).
- [13] J. M. Diego, *Constraining the abundance of primordial black holes with gravitational lensing of gravitational waves at LIGO frequencies*, [arXiv:1911.05736](#).
- [14] P. Schneider, J. Ehlers, and E. E. Falco, *Gravitational Lenses*. Springer Verlag, 1992.
- [15] L. S. Finn and D. F. Chernoff, *Observing binary inspiral in gravitational radiation: One interferometer*, *Phys. Rev.* **D47** (1993) 2198–2219, [[gr-qc/9301003](#)].
- [16] M. Maggiore, *Gravitational Waves. Vol. 1: Theory and Experiments*. Oxford Master Series in Physics. Oxford University Press, 2007.
- [17] LIGO-Virgo, <https://dcc.ligo.org/LIGO-P1900011/public>, .
- [18] P. Torrey, S. Wellons, F. Machado, B. Griffen, D. Nelson, V. Rodriguez-Gomez, R. McKinnon, A. Pillepich, C.-P. Ma, M. Vogelsberger, V. Springel, and L. Hernquist, *An analysis of the evolving comoving number density of galaxies in hydrodynamical simulations*, *MNRAS* **454** (Dec, 2015) 2770–2786, [[arXiv:1507.01942](#)].
- [19] P. Torrey, *private communication*, 2019.
- [20] K. Belczynski, D. E. Holz, T. Bulik, and R. O’Shaughnessy, *The first gravitational-wave source from the isolated evolution of two 40-100 Msun stars*, *Nature* **534** (2016) 512, [[arXiv:1602.04531](#)].
- [21] J. J. Eldridge and E. R. Stanway, *BPASS predictions for Binary Black-Hole Mergers*, *Mon. Not. Roy. Astron. Soc.* **462** (2016), no. 3 3302–3313, [[arXiv:1602.03790](#)].
- [22] D. Wysocki, D. Gerosa, R. O’Shaughnessy, K. Belczynski, W. Gladysz, E. Berti, M. Kesden, and D. E. Holz, *Explaining LIGO’s observations via isolated binary evolution with natal kicks*, *Phys. Rev.* **D97** (2018), no. 4 043014, [[arXiv:1709.01943](#)].
- [23] I. Dvorkin, J.-P. Uzan, E. Vangioni, and J. Silk, *Exploring stellar evolution with gravitational-wave observations*, *Mon. Not. Roy. Astron. Soc.* **479** (2018), no. 1 121–129, [[arXiv:1709.09197](#)].
- [24] M. U. Kruckow, T. M. Tauris, N. Langer, M. Kramer, and R. G. Izzard, *Progenitors of gravitational wave mergers: Binary evolution with the stellar grid-based code ComBinE*, *Mon. Not. Roy. Astron. Soc.* **481** (2018), no. 2 1908–1949, [[arXiv:1801.05433](#)].
- [25] M. Spera, M. Mapelli, N. Giacobbo, A. A. Trani, A. Bressan, and G. Costa, *Merging black hole binaries with the SEVN code*, [arXiv:1809.04605](#).
- [26] M. Mapelli, N. Giacobbo, F. Santoliquido, and M. C. Artale, *The properties of merging black holes and neutron stars across cosmic time*, *Mon. Not. Roy. Astron. Soc.* **487** (2019), no. 1 2–13, [[arXiv:1902.01419](#)].
- [27] C. L. Rodriguez, M. Zevin, P. Amaro-Seoane, S. Chatterjee, K. Kremer, F. A. Rasio, and C. S. Ye, *Black holes: The next generation—repeated mergers in dense star clusters and their gravitational-wave properties*, *Phys. Rev.* **D100** (2019), no. 4 043027, [[arXiv:1906.10260](#)].
- [28] S. Stevenson, M. Sampson, J. Powell, A. Vigna-Gómez, C. J. Neijssel, D. Szécsi, and I. Mandel, *The impact of pair-instability mass loss on the binary black hole mass distribution*, [arXiv:1904.02821](#).
- [29] G. Fragione, N. Leigh, and R. Perna, *Black hole and neutron star mergers in Galactic Nuclei: the role of triples*, *Mon. Not. Roy. Astron. Soc.* **488** (2019), no. 2 2825–2835, [[arXiv:1903.09160](#)].

- [30] **LIGO Scientific, Virgo** Collaboration, B. P. Abbott et al., *Binary Black Hole Population Properties Inferred from the First and Second Observing Runs of Advanced LIGO and Advanced Virgo*, *Astrophys. J.* **882** (2019), no. 2 L24, [[arXiv:1811.12940](#)].
- [31] E. Vangioni, K. A. Olive, T. Prestegard, J. Silk, P. Petitjean, and V. Mandic, *The Impact of Star Formation and Gamma-Ray Burst Rates at High Redshift on Cosmic Chemical Evolution and Reionization*, *Mon. Not. Roy. Astron. Soc.* **447** (2015) 2575, [[arXiv:1409.2462](#)].
- [32] P. Ajith et al., *Inspiral-merger-ringdown waveforms for black-hole binaries with non-precessing spins*, *Phys. Rev. Lett.* **106** (2011) 241101, [[arXiv:0909.2867](#)].
- [33] LSC, *L1 calibrated sensitivity spectra aug 06 2017*, tech. rep., <https://dcc.ligo.org/LIGO-G1801952/public>, 2017.
- [34] LSC, *H1 calibrated sensitivity spectra june 10 2017*, tech. rep., <https://dcc.ligo.org/LIGO-G1801950/public>, 2017.
- [35] LSC, *Unofficial sensitivity curves for various detector configurations used in iswp 2016*, tech. rep., <https://dcc.ligo.org/LIGO-T1500293/public>, 2016.